

Determination of spectroscopic parameters for 313 M dwarf stars from their APOGEE Data Release 16 H-band spectra

Pedro Sarmento^{1,2}, Bárbara Rojas-Ayala³, Elisa Delgado Mena¹, and Sergi Blanco-Cuaresma⁴

¹ Instituto de Astrofísica e Ciências do Espaço, Universidade do Porto, CAUP, Rua das Estrelas, PT4150-762 Porto, Portugal e-mail: pedro.sarmento@astro.up.pt

² Departamento de Física e Astronomia, Faculdade de Ciências, Universidade do Porto, Portugal

³ Instituto de Alta Investigación, Universidad de Tarapacá, Casilla 7D, Arica, Chile

⁴ Harvard-Smithsonian Center for Astrophysics, 60 Garden Street, Cambridge, MA 02138, USA

March 9, 2021

ABSTRACT

Context. The scientific community's interest on the stellar parameters of M dwarfs has been increasing over the last few years, with potential applications ranging from galactic characterization to exoplanet detection.

Aims. The main motivation for this work is to develop an alternative and objective method to derive stellar parameters for M dwarfs using the H-band spectra provided by the Apache Point Observatory Galactic Evolution Experiment (APOGEE).

Methods. Synthetic spectra generated with *iSpec*, *Turbospectrum*, *MARCS* models atmospheres and a custom made line list including over 1 000 000 water lines, are compared to APOGEE observations, and parameters are determined through χ^2 minimization.

Results. Spectroscopic parameters (T_{eff} , $[M/H]$, $\log g$, v_{mic}) are presented for a sample of 313 M dwarfs, obtained from their APOGEE H-band spectra. The generated synthetic spectra reproduce observed spectra to a high accuracy level. The impact of the spectra normalization on the results are analyzed as well.

Conclusions. Our output parameters are compared with the ones obtained with APOGEE Stellar Parameter and Chemical Abundances Pipeline (ASPCAP) for the same stellar spectrum, and we find that the values agree within the expected uncertainties. Comparisons with other previous near-infrared and optical literature are also available, with median differences within our estimated uncertainties found in most cases. Possible reasons for these differences are explored. The full H-band line list, the line selection for the synthesis, and the synthesized spectra are available for download, as are the calculated stellar parameters.

Key words. stars: fundamental parameters - stars: M dwarfs - techniques: spectroscopy

1. Introduction

M dwarfs are main sequence stars with masses ranging from $0.6 M_{\odot} \geq M_* \geq 0.08 M_{\odot}$, radii between $0.6 R_{\odot} \geq R_* \geq 0.1 R_{\odot}$, and T_{eff} from $3800 K \geq T_{\text{eff}} \geq 2300 K$ (Delfosse et al. 2000). They are the most abundant stars in the universe, with about 7 in every 10 stars in the Milky Way being M dwarfs, and accounting for most of its mass (Henry et al. 2006). M dwarfs are the faintest main-sequence stars, with the largest and brightest of them having only $0.1 L_{\odot}$. However, and despite their relative dimness, M dwarfs can be the key to a bright future in areas of astronomy such as galactic chemical evolution and exoplanet science.

As M dwarfs have a longer lifespan than other larger and brighter main-sequence stars and they represent such a large fraction of existing stars in our galaxy, M dwarf characterization is essential for our understanding of the galactic history. Some examples are Lépine et al. (2007), which uses spectroscopic indices and the kinematic measurements of both disk dwarfs and halo subdwarfs to revise metallicity classes for these objects, and Bochanski et al. (2007), that uses a spectroscopic sample of low-mass stars to investigate the properties of the thin and thick disks.

M dwarfs are very good targets for surveys dedicated to the discovery of Earth-like planets. Due to their faintness, their habitable zone is much closer to the star than it is for solar-type stars, and, due to their small radius and mass, the relative difference in

size between any potential exoplanet and the host star is much smaller than for more massive stars. As the two most successful current methods for planet detection, radial velocity and transit, are indirect methods, this means that detecting exoplanets in the star's habitable zone is orders of magnitude easier for M dwarfs than for solar-type stars. Several programs therefore focus primarily on finding potentially habitable planets around M dwarfs, such as MEarths (Irwin et al. 2014), and CARMENES (Alonso-Floriano et al. 2015) or HARPS (Bonfils et al. 2013), among others, have also targeted M dwarfs with the purpose of planet detection. There have also been many studies detailing how life might be possible in planets around M dwarfs (e.g. Segura et al. 2005; Scalo et al. 2007; France et al. 2013).

Stellar characterization through spectroscopy can provide the scientific community with fundamental stellar parameters such as effective temperature, metallicity, and surface gravity. These stellar parameters can be used, for example, to discover more information about the history of our galaxy through the study of metal-poor stars (Suda et al. 2008), improve our understanding of giant stars (Ness et al. 2016) or for the characterization of exoplanet host stars, and, indirectly, of exoplanets (e.g. Sousa et al. 2011; Santos et al. 2013).

Spectroscopic analysis of M dwarfs in the NIR has been a developing topic over the last few years, with works in lower resolution such as Rojas-Ayala et al. (2010, 2012), a characterization of 133 M dwarfs using K-band (2.0-2.4 micron, $S/N > 200$,

$R \sim 2700$) spectra, as well as Mann et al. (2013)'s work with $1300 < R < 2000$ optical and infrared spectra, and Terrien et al. (2015)'s catalog of 886 M Dwarfs in the full NIR (0.8–2.4 micron, $R \sim 2000$). More recently, works have moved to higher resolution, with publications such as Veyette et al. (2017) providing an analysis of 29 M dwarfs from their NIRSPEC (Keck II) Y-band ($\sim 1\mu m$, $R \sim 25\,000$) spectra with the help of PHOENIX models. The high-resolution studies of Önehag et al. (2012), using CRIRES $R \sim 50\,000$ J band spectra, as well as the more recent Passegger et al. (2019)'s characterization of 300 stars by fitting PHOENIX models to their high-resolution ($R = 80\,000$ – $100\,000$) CARMENES optical and near-infrared spectra expanded our understanding of the spectra of these stars.

Our work positions itself as a continuation and extension of these works, providing a new pipeline for spectroscopic parameter derivation from the Apache Point Observatory Galactic Evolution Experiment (APOGEE, Majewski et al. 2017)'s mid-high resolution ($R \sim 22\,000$) H-band (1.5–1.7 micron) stellar spectra.

This paper is structured as follows: Section 2 contains a description of both APOGEE and our sample stars, detailing available previous literature analysis of them; Section 3 details the methodology used for our characterization of stellar spectra; Section 4 contains our main results, including both an H-R diagram of our 313 characterized stars and an example of a synthesized stellar spectrum; Section 5 includes our analysis of the derived parameters, including literature comparisons; and Section 6 details our main conclusions and future possibilities for the pipeline.

This work comes as a follow-up to Sarmento et al. (2020), using similar methods and expanding the parameter space of its analysis into late-K and early-M dwarf stars.

2. Data

All M dwarf spectra used for stellar characterization in this paper comes from the APOGEE survey. APOGEE is an H-band (1.5–1.7 micron) Sloan Digital Sky Survey program that focuses on obtaining $R \sim 22\,500$ stellar spectra with a 300-fiber spectrograph. It is split between APOGEE-N, using the Sloan 2.5 m telescope at the Apache Point Observatory in New Mexico (Gunn et al. 2006), and APOGEE-S, which uses the 2.5 m duPont telescope at the Las Campanas Observatory in Chile (Bowen & Vaughan 1973). It targets mostly red giants and provides public spectra for more than 200 000 stars in its Data Release 14 (DR14, Holtzman et al. 2018). APOGEE has observed FGK and M dwarfs for calibration purposes or as part of ancillary programs (Zasowski et al. 2013).

Their spectroscopic parameters (effective temperature, surface gravity, microturbulence, macroturbulence, rotation, overall metal abundance $[M/H]$, relative α -element abundance $[\alpha/M]$ (determined by fitting simultaneously lines of O, Mg, Si, S, Ca, and Ti), carbon $[C/M]$, and nitrogen $[N/M]$ abundances) have been derived with APOGEE Stellar Parameter and Chemical Abundances Pipeline (ASPCAP, García Pérez et al. 2016). ASPCAP also determines abundance for 24 different elements. APOGEE's Data Release 16 (DR16, Ahumada et al. 2019, 2020; Jönsson et al. 2020) is the most recent release of APOGEE data, and it is the first one to include results obtained with APOGEE-2. The spectra for more than 430 000 stars is included in this data release. The previously released data was analyzed again, with small changes to the data processing and ASPCAP analysis procedures. Comparing with previous data releases, the most important of these changes is an expansion of the parameter space of the characterized stars, with published calibrated $\log g$ values up to $6.0\,dex$ rather than $4.5\,dex$, and T_{eff} down to $3200\,K$. ASPCAP works by searching and interpolating a grid of synthetic spectra to find the

best match for each observed spectrum, adopting the parameters of the synthetic spectrum as the preliminary parameters for each star. These parameters are then calibrated to follow the theoretical models, with the calibrated values being the final parameters for each star.

In addition to the spectra characterized by ASPCAP DR16, we decided to apply our method to the spectra of the same stars, as published in APOGEE DR14 (Holtzman et al. 2018). These results are included in the paper for reference and comparison between the two data releases, and because they were the main results of the first author's thesis. The main differences between the two data releases, in addition to small cleanups of the spectra, including the removal of cosmic rays, are the parameter calibrations, which, for $\log g$ and T_{eff} , are now extended to better characterize the M dwarf parameter range.

2.1. Sample selection

All stars in our sample were chosen as part of APOGEE's ancillary M dwarf program. The goal of this program was to constraint the rotational velocities and compositions of over 1400 M dwarfs and to detect their low mass companions through RV variability, as published in Deshpande et al. (2013). The targets are drawn primarily from two sources, the LSPM-North catalog of nearby stars (Lépine & Shara 2005) and the catalog of nearby M dwarfs by Lépine & Gaidos (2011). In order to obtain their final selection, magnitude and color cuts ($7 < H < 12$; $V - K > 5.0$; $0.4 < J - H < 0.65$; $0.1 < H - K_s < 0.42$) were applied to stars from those catalogs that fell on APOGEE's observation fields. In addition to both of these proper-motion selected catalogs, additional known planet hosts and other stars with available rotational speed, metallicity, or radial velocity estimates were also included for calibration purposes. Although Deshpande et al. (2013) published rotational velocities for these M dwarfs, they were unable to provide stellar parameters for all stars in the sample due to the inability to model the strong H_2O bands found in the spectra.

The sample analyzed in this work was filtered by $S/N > 200$ to remove the spectra with worst quality from the sample. We chose this value as a limit because it both provided us with enough stars to perform a statistical analysis and was not so large that the time for the computational analysis became unpractical. The distribution of APOGEE's reported S/N for the stars in our final sample is available in the bottom part of Fig. 1. In addition to our star selection by S/N , 21 additional stars characterized by Souto et al. (2020) and 9 stars with confirmed exoplanets were included in the sample, despite having a lower S/N ratio than the cutoff for the rest of our analyzed stars. In order to test the lower bounds of our method, 7 M dwarfs with ASPCAP $T_{\text{eff}} < 3000\,K$ were included in the sample as well. Our final M dwarf sample contains 313 stars.

2.2. Sample characterization

We display both the magnitude distribution and the APOGEE-estimated S/N of our 313 sample stars in Fig. 1. The figure shows how most of our sample has high S/N spectra, and also shows how fainter stars tend to have lower S/N as expected. The small clump of lower magnitude (4–6), $S/N < 300$ stars corresponds to the M dwarfs from Souto et al. (2020) that have been characterized with interferometry.

We display the location in the sky of all M dwarfs in the sample, showing both their Right Ascension (RA) and Declination (Dec) in Fig. 2. Most of the stars are located in the northern

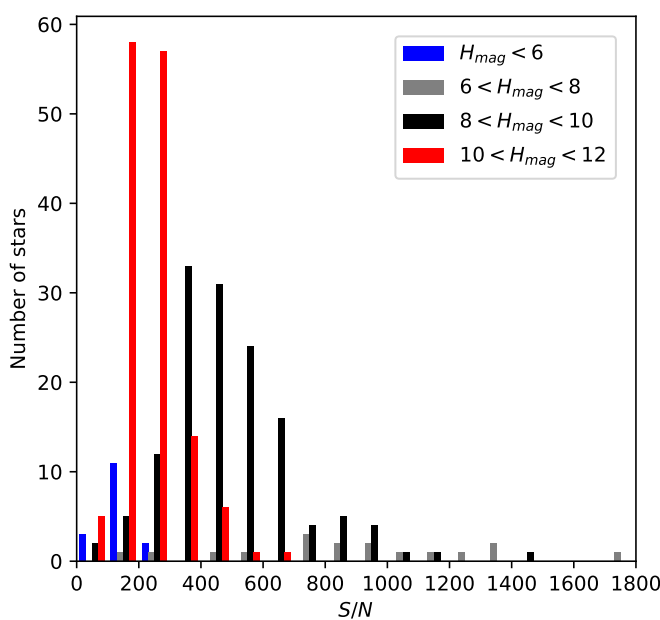


Fig. 1. Histogram presenting both the H magnitude and the S/N (from APOGEE) of our M dwarf sample stars.

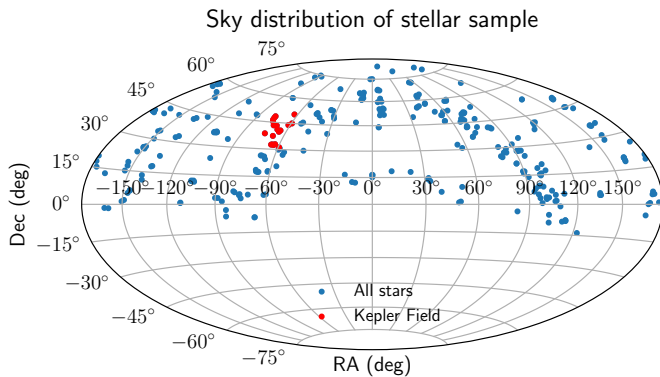


Fig. 2. Map showing the location in the sky of our sample M dwarfs. Kepler target field is highlighted in red.

hemisphere ($\text{Dec} > 0 \text{ deg}$), as they were observed by APOGEE-2N. Nineteen stars in our sample are located in the Kepler field (Latham et al. 2005), fourteen of which have been observed by the Kepler Space Telescope.

2.3. Available literature values for the sample

We cross-matched our M dwarf sample with different surveys and works related to spectroscopic stellar characterization. We found 8 works with stars in common with our sample that serve as our literature comparisons - ASPCAP (Garcia Pérez et al. 2016), Terrien et al. (2015), Gaidos et al. (2014), Hejazi et al. (2019), Souto et al. (2020), Passegger et al. (2019), Rajpurohit et al. (2018a) and Rajpurohit et al. (2018b). This subsection is dedicated to explanations of these works and their determined parameters for the stars in common between them and our M dwarf sample.

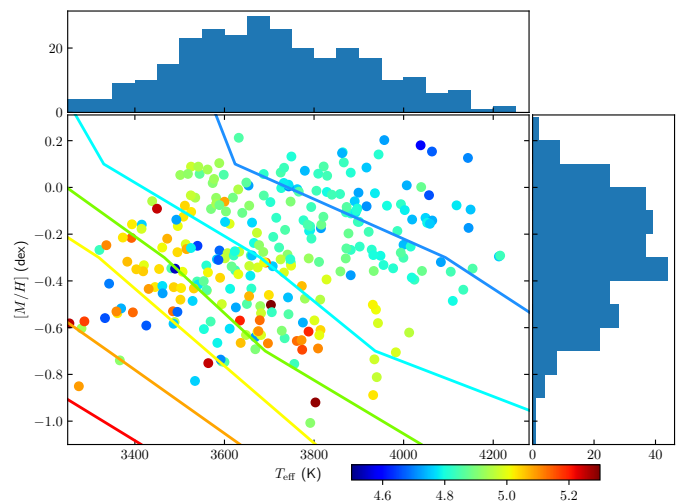


Fig. 3. ASPCAP T_{eff} and $[M/H]$ values for M dwarfs in sample, with overplotted PARSEC isochrones (Bressan et al. 2012) for an age of 5Gyr created with different $\log g$ values (scale is in dex). Points are color-coded based on the metallicity value derived for each star.

2.3.1. ASPCAP

ASPCAP (Garcia Pérez et al. 2016), as the pipeline dedicated to derivation of spectroscopic parameters for stars observed with APOGEE, published their estimates for stars in our sample as well. The ASPCAP pipeline provides both a preliminary set of output parameters for each observed star as well as a final set of calibrated parameters focused on its main target of giant stars. However, their calibrated parameter ranges do not include all M dwarfs in our sample, as their lower boundary for T_{eff} is 3200 K. Their values can still be an important reference for our pipeline, as they have been shown to be consistent by Schmidt et al. (2016), which performed an extensive analysis on both the T_{eff} and $[M/H]$ values ASPCAP produced for 3834 M dwarfs, comparing them to photometric and interferometric parameters for the same stars. Based on interferometric data from Boyajian et al. (2013), color- T_{eff} relations from Mann et al. (2015), and the infrared flux technique published by Casagrande et al. (2008), they concluded that the ASPCAP T_{eff} is accurate to about 100 K for stars between 3550–4200 K, and $[M/H]$ values are accurate to about 0.18 dex. This means that, despite ASPCAP's main focus being on giant stars and not M dwarfs, we can take their measurements of T_{eff} and $[M/H]$ as consistent for the parameters of M dwarfs in our sample, and we will thus use them as a comparison value for our analysis.

From the 313 stars in our sample, ASPCAP has published their final, calibrated $[M/H]$, T_{eff} , and $\log g$ for 283 stars. These values are displayed in Fig. 3, with the color indicating the ASPCAP $\log g$ values for each star. The figures shows that their T_{eff} values are concentrated around 3600–3800 K, and $[M/H]$ are between -0.4 and +0.0 dex. The metallicity distribution follows an approximate Gaussian shape, with an average value of -0.29 dex and a standard deviation of 0.27 dex. These results show that a significant fraction of stars in our sample are early M dwarfs. According to ASPCAP results, our sample is, on average, more metal-poor than the solar neighborhood, which has mean metallicity values around -0.20 dex (Holmberg et al. 2007).

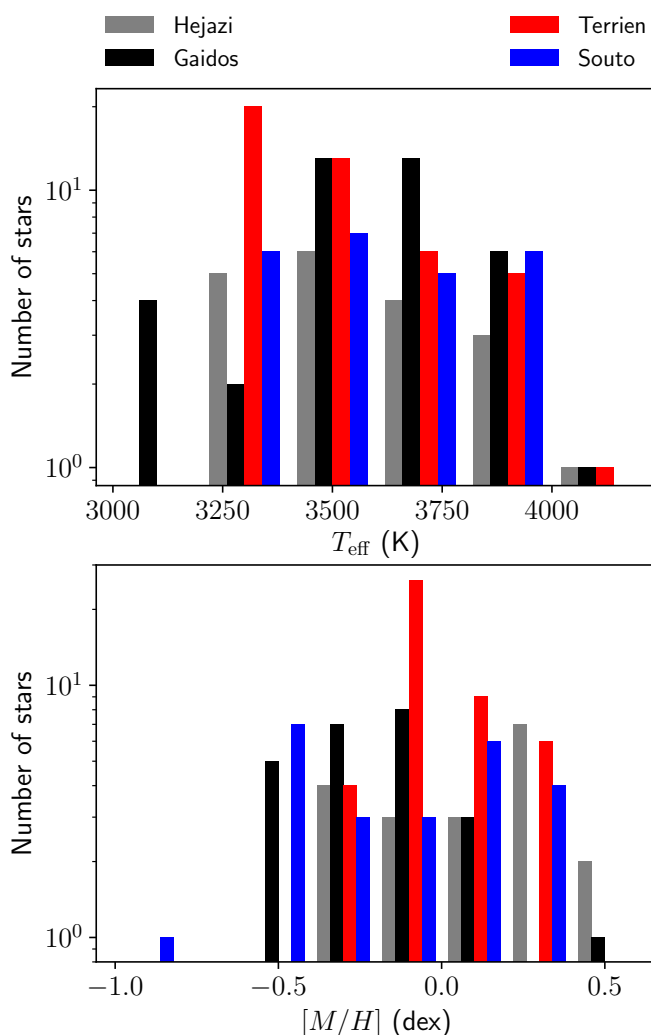


Fig. 4. T_{eff} (TOP, a) and $[M/H]$ (BOTTOM, b) values from 4 literature sources: Gaidos et al. (2014) (black, T_{eff} for 40 stars, $[Fe/H]$ for 24 stars), Hejazi et al. (2019) (orange, filled bars, 19 stars), Terrien et al. (2015) (red, 45 stars), and an aggregate between Souto et al. (2017), Souto et al. (2018), and Souto et al. (2020) (blue, 24 stars). Number of stars is displayed with logarithmic notation for visibility.

2.3.2. Terrien et al. (2015)

From the 886 stars characterized in Terrien et al. (2015), 45 are included in our sample. Their spectra have wide coverage ($0.8 - 2.4 \mu\text{m}$) but low resolution ($R \sim 2000$). Their T_{eff} values are determined by analysis of water indices in the K band and have uncertainties above 100 K, and their $[M/H]$ values are measured using empirical spectroscopical calibrations with uncertainties around 0.12 dex. Their published parameters are shown in Fig. 4. Comparing their parameter distribution with the full ASPCAP sample, we find that Terrien et al. (2015) is more representative of later-type M dwarfs, having a significant fraction of stars with published T_{eff} between 3200–3500 K.

2.3.3. Souto et al. (2017), Souto et al. (2018), Souto et al. (2020)

We find that some of the best characterized stars in the APOGEE sample are the M dwarfs that were analyzed by Souto et al. (2017), Souto et al. (2018), and Souto et al. (2020). That is because these

works use spectral synthesis and a combination of MARCS and PHOENIX model atmospheres to determine both stellar parameters and chemical abundances for 8 different elements using APOGEE spectra. Their reported uncertainties are $T_{\text{eff}} \pm 100$ K, $\log g \pm 0.2$ dex and $[Fe/H] \pm 0.1$ dex. A total of 24 different M dwarfs were characterized by this method - Kepler 138 and Kepler 186 in Souto et al. (2017), Ross 128 in Souto et al. (2018), and 21 other stars in Souto et al. (2020). Among all the stars in our sample previously characterized in the literature, the most metal-poor one is 2M03150093+0103083, with $[Fe/H] = -0.91$ dex, and it was characterized by Souto et al. (2020).

2.3.4. Gaidos et al. (2014)

Gaidos et al. (2014) analyzed optical spectra of nearby K and M dwarfs with $R \sim 1000$ and determined their spectroscopic parameters by fitting model spectra to observations. Their estimated errors vary between stars, but are around 100 K for T_{eff} and 0.12 dex for $[Fe/H]$. From the 2970 stars with $d < 50$ pc observed by Gaidos et al. (2014), 28 are included in our sample, and their parameters are shown in Fig. 4. The reduced number of stars, combined with the lack of $[Fe/H]$ available for half the stars in the sample, does not allow for an extensive statistical analysis of this stellar subsample. Nevertheless, it is possible to notice Gaidos et al. (2014) reported T_{eff} values between 3100–3500 K for a greater number of stars in this subsample than in the main ASPCAP one, helping us characterize the lower T_{eff} stars in our sample. Gaidos et al. (2014) also found metallicity for stars in our sample across a larger parameter space ($-0.6 < [Fe/H] < +0.4$ dex) than ASPCAP.

2.3.5. Hejazi et al. (2019)

Hejazi et al. (2019) published chemical properties for 1544 high proper-motion M dwarfs and subdwarfs from low-mid resolution ($\sim 2000 - 4000$) optical spectra. A template-fit method was developed, based on the measurement of TiO and CaH molecular bands near 7000 Å. The analysis of 48 binary systems suggests precision levels of ± 0.22 for $[M/H]$, ± 0.08 for $[\alpha/Fe]$, and ± 0.16 for the combined index $[M/H] + [\alpha/Fe]$. We find 19 stars in common between our observed sample and their study. From Fig. 4, we can verify that the characterized stars are dispersed across a wide range of temperatures, with a stronger concentration of stars around $T_{\text{eff}} = 3600$ K. As for the metallicities, we find stars both above and below solar neighborhood values, but no star within $-0.1 < [M/H] < +0.1$ dex, which must be considered when comparing our results to theirs.

2.3.6. Passegger et al. (2019)

We cross-matched our sample with the 300 stars characterized by Passegger et al. (2019) and found 14 stars in common. As mentioned in Section 1, this work derived parameters for M dwarfs by using a χ^2 to fit PHOENIX-SESAM models to high-resolution ($R \sim 90\,000$) CARMENES spectra in both the visible and infrared wavelength ranges. Their reported uncertainties depend on each star's rotational velocity and, for NIR spectra, are as low as 51 K for T_{eff} , 0.07 for $\log g$, and 0.16 for $[Fe/H]$.

2.3.7. Rajpurohit et al. (2018a)

Another study with CARMENES spectra is Rajpurohit et al. (2018a). This work focused on matching BT-Settl model spectra

to CARMENES optical and near-infrared observations of 292 M dwarf spectra. Since this work determines parameters by matching observed spectra to a grid of previously computed models, the reported uncertainties correspond to the size of the grid, 100 K for T_{eff} and 0.1 dex for both $\log g$ and $[M/H]$. We find 12 stars in common between our sample and the one characterized by Rajpurohit et al. (2018a), which are part of the 14 stars later characterized by Passegger et al. (2019) and listed in section 2.3.6.

2.3.8. Rajpurohit et al. (2018b)

The same technique was applied to 45 M dwarfs observed with APOGEE in Rajpurohit et al. (2018b). We have 8 stars in common, with six of them having $T_{\text{eff}} < 3300$ K and are some of the coldest stars in our sample. The reported uncertainties for the parameters of these stars are $T_{\text{eff}} \pm 100$ K, $\log g \pm 0.3 - 0.5$ dex and $[M/H] \pm 0.05$ dex. A comparison between our derived parameters and the previously available parameters for these stars is available in Fig.13.

We found López-Valdivia et al. (2019) as an example of another large scale, high resolution study of spectroscopical parameters for M dwarfs in the infrared, but, unfortunately, it shares no stars in common with APOGEE. The best spectroscopic parameters available in literature for our sample stars are the ones cited in this section and ASPCAP values. Therefore, comparisons between our results and literature values are made against the works mentioned above.

3. Methodology

This section includes the steps in our method that are specific for M dwarfs. The full rundown of our pipeline is available at Sarmento et al. (2020). Summarizing, our first step is to normalize the APOGEE observed spectra for each star using the template method and a synthetic spectrum. Then, we created custom software that uses *iSpec* (Blanco-Cuaresma et al. 2014; Blanco-Cuaresma 2019) and *Turbospectrum* (Alvarez & Plez 1998; Plez 2012) to derive the atmospheric parameters through a χ^2 minimization algorithm that compares observed and synthetic spectra. These synthetic spectra are created using MARCS (Gustafsson et al. 2008) stellar atmospheric models and a custom line list. The best fitting synthetic spectra are selected through χ^2 minimization, using MPFIT (Markwardt 2009) internally through *iSpec*. Finally, the parameters of the best matching synthetic spectra are taken as our measurements for the stellar parameters of each star.

We created routines for the download, format conversion, normalization of the sample spectra, and have made the pipeline as automated as possible, but the χ^2 minimization and the synthesis of the best fitting spectra are done with *Turbospectrum*, controlled by *iSpec* python code. The custom routines are programmed in Python 3 and for the 2020 distribution of *iSpec*. They are included in a public repository together with the full results, line lists, line masks, and everything required to replicate the process described in this paper.

3.1. Line list

The line list used for M dwarf spectral syntheses is more complex than the one used for the spectra of FGK stars, as these stars have many water (H_2O) lines that are not visible in hotter stars. These water lines form a thick blanket that makes the flux continuum

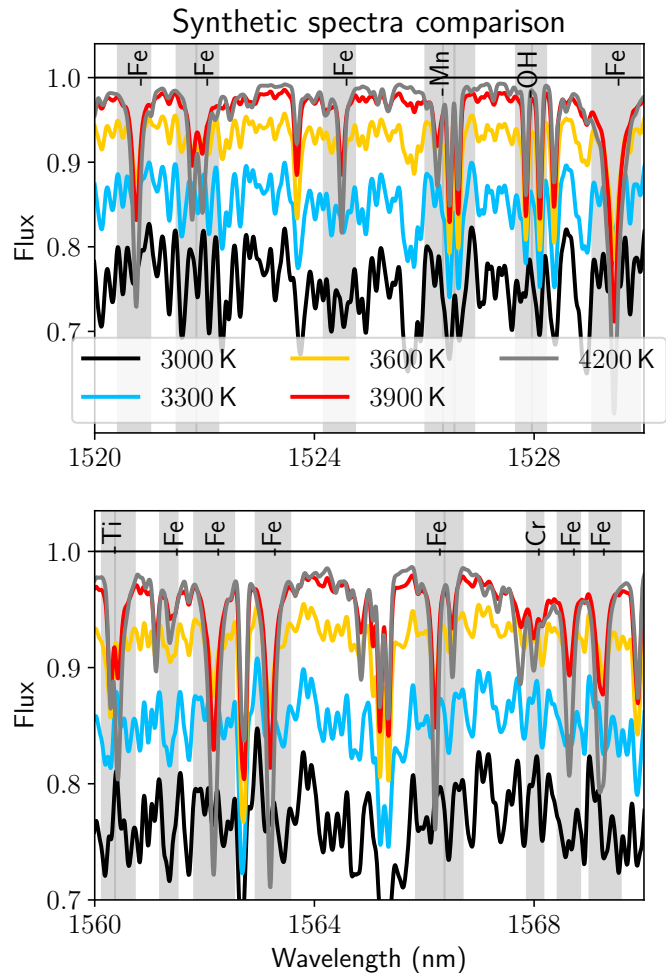


Fig. 5. Comparison between synthetic spectra made with different T_{eff} . The spectra corresponds to synthesis made with T_{eff} 4200K (gray), 3900K (red), 3600K (orange), 3300K (orange) and 3000K (black).

harder to identify, as shown in figure 5. We use the water line list first published in Barber et al. (2006), retrieved from Bertrand Plez's personal website¹. We note here that a more recent work on water lines has been published by Polyansky et al. (2018), but preference was given to usage of the water line list from Barber et al. (2006) as it was already formatted for Turbospectrum and of a more computationally manageable size. A total of 1 263 825 water lines were included in the M dwarf line list, along with the 85334 lines from other molecules and atoms already available at Sarmento et al. (2020), made from a combination of the Vienna Atomic Line Database (VALD, Piskunov et al. 1995) and the APOGEE line list (Shetrone et al. 2015). This resulted in a final list of 1 349 159 lines.

3.2. Spectra Normalization

As we can see in Fig.5, a 300 K difference in T_{eff} can mean a 0.05 difference in the continuum flux for a star, which is enough to turn an accurate fit into a terrible one. Therefore, in order to accurately normalize an M dwarf's H-band spectrum, an accurate initial input stellar T_{eff} for that star is required. Normalizations with templates synthesized with T_{eff} closer to the star's real T_{eff} will result in continuum values closer to the real ones, meaning

¹ <http://www.pages-perso-bertrand-plez.univ-montp2.fr/>

the synthetic spectra will closely resemble the observed ones. Therefore, the first important step towards deriving a star's atmospheric parameters is to have good estimates for their T_{eff} and metallicity.

Given the lack of a consistent literature source for the T_{eff} of our sample stars, and in order to minimize the effect of the visual choice of T_{eff} based on the normalized spectra, the spectrum of each star in our sample was normalized using synthetic spectra with 148 different combinations of T_{eff} , $\log g$ and $[M/H]$, corresponding to values taken from PARSEC isochrones (Bressan et al. 2012) for stars with ages between 10^9 and 10^{10} years. This approach is done to avoid unrealistic combinations of output parameters. We selected isochrones with a 0.2 dex spacing in $[M/H]$ values, rounding T_{eff} values to the nearest multiple of 100 K, and $\log g$ being rounded to the nearest multiple of 0.1 dex. These values are selected to both have an amount of normalizations that can be computationally generated in a short amount of time and to have an even distribution across our expected parameter space for M dwarfs, as our sample stars are expected to have parameters approximating one of these combinations. The full list of parameter combinations is available at appendix A.

Afterwards, we compared each of the normalized spectra to the template used to create the normalization. By calculating and minimizing the χ^2 across our line mask region (see section 3.3) between the observed and the template spectra, the parameters for the best normalization template are defined. Fig. 6 displays the χ^2 values for different normalization parameters for star 2M05201152+2457212. That figure shows how the χ^2 values depend strongly on the normalization template, and can indicate the quality of the template choice for normalization. It is also clear that templates with similar parameters have similar χ^2 values. This fact shows that these values are close to the real stellar parameters, and the normalization with a template with $T_{\text{eff}} = 3700$ K, $\log g = 4.7$ dex, $[M/H] = 0.0$ dex can be used for this star in the next steps of the pipeline.

3.3. Line mask

As explained in Sarmento et al. (2020), a line mask instructs *iSpec* on which spectral regions should be considered for comparing observed and synthetic spectra. A line mask specifically made for M dwarf stars was therefore required for the code to match an appropriate model to the observations. The star Ross128 (2M11474440+0048164), as an APOGEE M-dwarf with $S/N \sim 229$ that has previously been characterized by Souto et al. (2018), was chosen as the basis for this line mask. A synthetic spectrum was generated using the parameters found for the star by Souto et al. (2018) ($T_{\text{eff}} = 3231$ K, $[Fe/H] = 0.03$ dex and $\log g = 4.96$ dex). This synthetic spectrum was used to normalize the observed one and then compare it. Regions and spectral lines with a good agreement between both spectra were selected for the line mask displayed in Fig. 7. The areas where the synthesis did not reproduce well the observed spectrum were discarded to create the final line mask shown. We note that, despite the slight errors in the Al lines around 1675 nm, we included these lines in our line mask. This was done because the two Al lines are the strongest lines we find across our wavelength range, and they are very well reproduced across other stars (see for example the appendix for Figs.B.2, B.3, B.4).

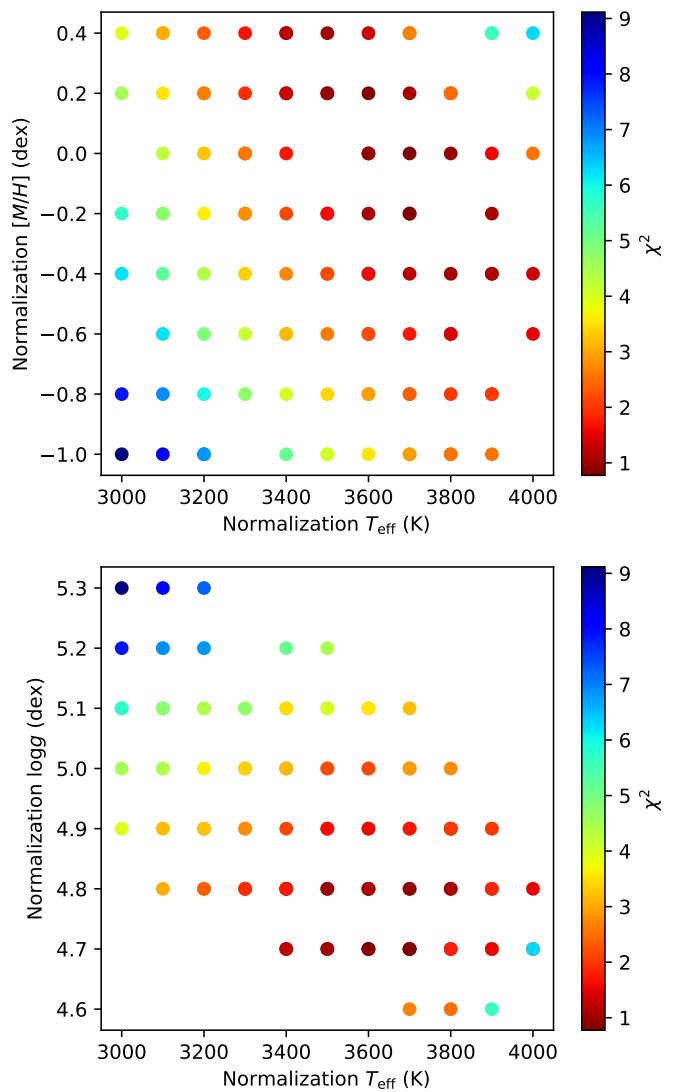


Fig. 6. TOP (a): Scatter plot displaying the χ^2 values measured for different T_{eff} and metallicity combinations for templates for the normalization of star 2M05201152+2457212. BOTTOM (b): Similar plot with T_{eff} and $\log g$ for the same star.

3.4. Free parameters

The free parameters used for the syntheses of M dwarf spectra are the same as the ones used in Sarmento et al. (2020) for the syntheses of the spectra of FGK stars - effective temperature (T_{eff}), surface gravity ($\log g$), metallicity ($[M/H]$), micro-turbulent velocity (v_{mic}), projected rotational velocity ($v \sin i$), and spectral resolution. The input values used are, for T_{eff} , $\log g$, and $[M/H]$, the ones used to create the template spectra for the normalization (see Section 3.2). The initial values for the remaining free parameters are 1.06 km/s for the v_{mic} , 1.6 km/s for $v \sin i$, and 22 000 for the resolution. We note that, despite leaving the resolution as a free parameter, our output values for this parameter are close to 22 000.

However, an important change required to keep the output parameters limited to realistic values is the restriction of possible output parameters to a given parameter space. Restricting the parameters to a given interval based on the starting values allows the code to both take the first guess given by the normalization template into account and at the same time allowing it to fine-tune

the parameters towards optimal values for χ^2 minimization. The output parameters are limited to the initial template parameters ± 350 K (for T_{eff}), ± 0.2 dex ($\log g$) and ± 0.3 dex ($[M/H]$). We found these ranges through trial and error, and testing the method with multiple stars. They are a balance between the information given by the normalization template and the freedom required for the pipeline to find the best fit for a given spectrum.

3.5. Error estimation

Due to the way our pipeline is setup, we have two major possible error sources, one associated to a poor choice of normalization, and one connected to Turbospectrum and the derivation of the best fit synthetic spectrum for each star. In this section, we will try to quantify the errors associated to both of these sources across our M dwarf parameter space.

3.5.1. Normalization template errors

As the shape of the characterized spectra, and consequent derived parameters, are strongly influenced by the normalization template used, we decided to test our pipeline by running multiple normalizations for the same observed star. A sample of 4 test stars was selected, covering a wide range of stellar parameters. For each test star, we ran the pipeline with all normalization templates with χ^2 within a 10% margin from the best templates found for each star, using the χ^2 values as an indication that the template is appropriate for the studied star. We ran the pipeline 20 times for each normalization template, injecting Gaussian errors proportional to the S/N . The errors are injected so the deterministic pipeline does not return the same output parameters on every iteration, allowing us to know how the parameters can change across multiple observations of the same star. We do note here that these tests result in an underestimation of the actual errors, as errors affecting the continuum normalization will produce correlations across multiple pixels. Therefore these serve as a minimum estimate for the actual errors in our measurements. Table 1 summarizes our results for a test sample of 4 stars, including the average and standard deviation obtained across the 20 runs of the pipeline for each normalization template per star.

The results displayed demonstrate that the output parameters can vary significantly with the template used for the normalization of the spectra. They also demonstrate the difficulty in assessing which template works best for a given star, as χ^2 values can be very similar even for spectra with varying parameters. The standard deviation verified within the same template used also shows the consistency of the pipeline itself for a given spectrum, which is further explored in the following section.

3.5.2. Errors associated with S/N

In order to estimate the errors associated with the S/N inherent to the spectra and the method used to find the best fit for each normalized spectra, a sample of 20 M dwarfs with different S/N and stellar parameters was selected. The pipeline was ran 20 times per star, with Gaussian errors proportional to the reported S/N of each star injected into the observed spectra before normalizing them with the method described in Section 3.2. Similar to the tests described in Section 3.5.1, these are also underestimations of the possible errors, as only uncertainties associated with individual pixels are taken into account. In order to have a more statistically relevant sample size, 80 additional iterations of the pipeline were run for each of 4 selected stars that cover a wide parameter range,

for a total of 100 pipeline iterations per star. The results of these tests are summarized in Table 2.

As shown in the table, the output of the pipeline is very consistent across multiple iterations, with T_{eff} having standard deviations below 12 K, $[M/H] < 0.03$ dex and $\log g < 0.09$ dex for all analyzed stars. There is no strong S/N effect on the standard deviation measured, as the values remain very consistent across all stars in the sample. These tests suggest that most of the possible errors in the final results are a result of the templates used for the normalization of each observed spectrum, and showing that $\log g$ is the parameter with the largest associated error.

Given the errors measured in the displayed tests and the size of the grid used for the selection of the normalization template, we estimate the overall errors of our pipeline to be around $T_{\text{eff}} \pm 100$ K, $[M/H] \pm 0.1$ dex and $\log g \pm 0.2$ dex, with a large percentage of these errors coming from the inherent uncertainty in the choice of normalization template used for a given star. This choice is limited by the PARSEC evolutionary code, as it is the only one publicly available covering the M dwarf parameter space with a good range coverage. Another possible error source can be the line mask used for the χ^2 calculation, as χ^2 values can be very similar for different normalization templates and changes in the line mask can result in the selection of different templates as well.

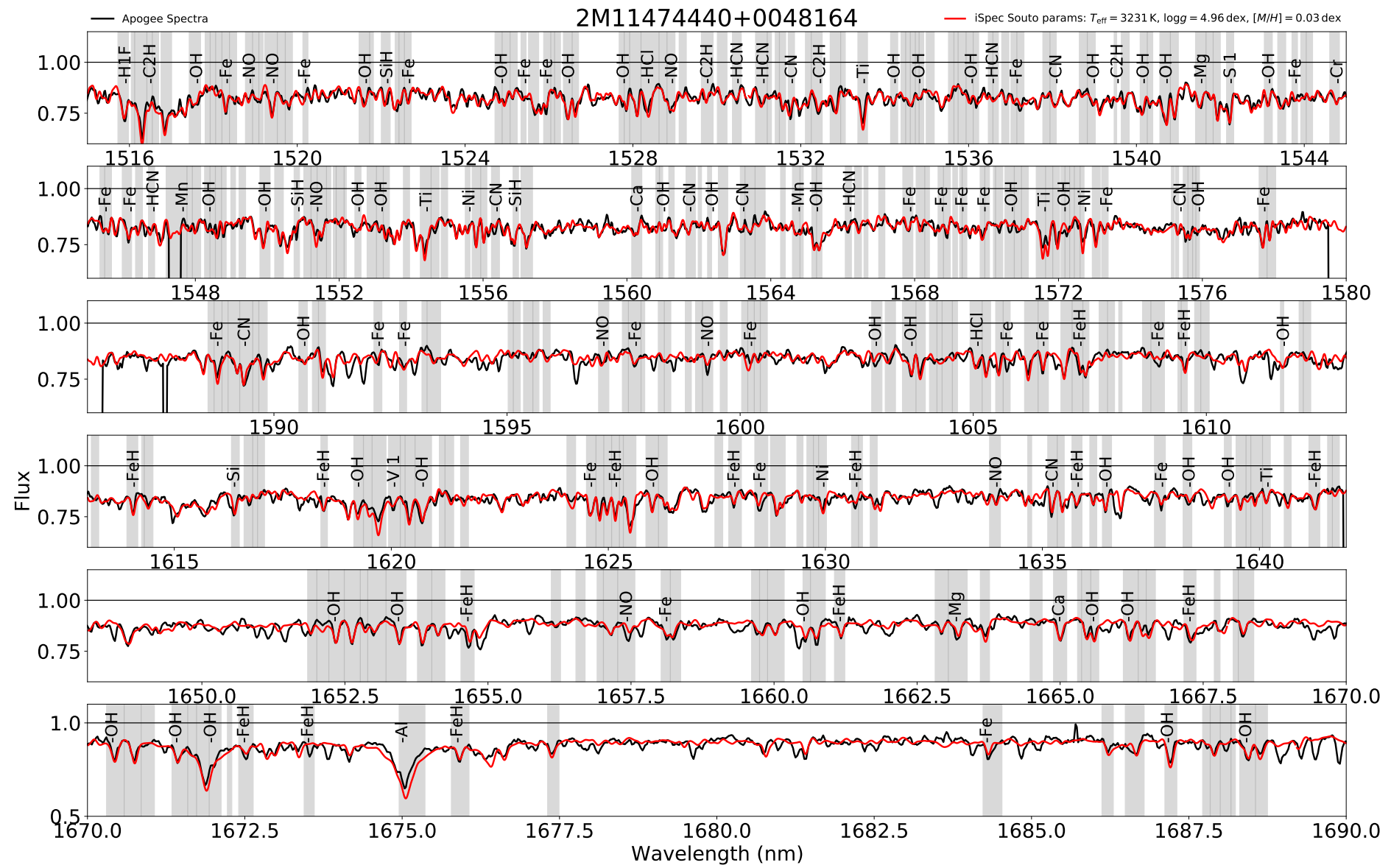


Fig. 7. Comparison between the observed spectrum of Ross 128 (2MASS J11474440+0048164), normalized using the template method (black), and a synthetic spectrum created using the literature (Souto et al. 2018) parameters for that star (red). The parameters used to generate the synthetic spectrum were $T_{\text{eff}} = 3231 \text{ K}$, $\log g = 4.96 \text{ dex}$, $[M/H] = +0.03 \text{ dex}$. The ASPCAP preliminary parameters for this star are $T_{\text{eff}} = 3212 \text{ K}$, $\log g = 4.45 \text{ dex}$, $[M/H] = -0.60 \text{ dex}$. The areas in gray represent the ones included in the line mask created from these spectra.

3.6. Summary

This section contains a small summary of the steps required to derive M dwarf stellar parameters using our pipeline.

- 144 different synthetic spectra are generated using parameter combinations taken from PARSEC isochrones and expected for M dwarfs. We note that the MARCS models in this parameter space are provided in steps of 100K for T_{eff} , 0.25 dex for $[Fe/H]$, and 0.5 dex for $\log g$, and we interpolate between them to create the grid whenever necessary. This interpolation is done entirely within *iSpec*, and we have not edited that part of the code.
- The observed combined spectrum for each sample star is downloaded from APOGEE, and normalized using each of the previously generated synthetic template spectra.
- The best normalization template for each star is chosen based on a χ^2 comparison between each template and its resulting normalized spectrum.
- *iSpec* (Blanco-Cuaresma et al. 2014; Blanco-Cuaresma 2019), as a shell for *Turbospectrum* (Alvarez & Plez 1998; Plez 2012), is used to generate synthetic spectra from a set of starting values. These synthetic spectra are created using *MARCS* (Gustafsson et al. 2008) stellar atmospheric models and a custom line list.
- Specific line masks are required for the synthesis of spectrum of stars with different spectral types, and they include the most relevant wavelength areas for spectral parameter determination.
- The synthetic spectra are matched to the normalized observed ones through a χ^2 minimization algorithm based on MPFIT (Markwardt 2009). The algorithm runs on a list of previously selected wavelength regions defined as the line mask.
- χ^2 minimization is used to find the best match between a synthetic spectrum and a given observed one, interpolating the available *MARCS* whenever necessary. Then, the spectral parameters used to generate the synthetic spectrum are taken as corresponding to the observed star.

4. Results

The spectra of the 313 M dwarfs in our sample were analyzed with the method detailed in Section 3, and the derived T_{eff} , $\log g$ and $[M/H]$ are plotted in Figs. 8 and 9. The full results are available at the appendix, in Table C.1. The errors included in the plots are ± 100 K for the T_{eff} , $\log g \pm 0.2$ dex, and $[M/H] \pm 0.1$ dex. Fig. 10 includes the parameters derived with APOGEE DR14, and the full list of parameters derived with that Data Release is included in Table D.1, in the appendix.

The isochrone comparisons presented in Fig. 8 show that, as expected, for most of the sample, our methodology's output T_{eff} and $\log g$ agree with the values predicted by the PARSEC models for M dwarfs. Despite this, the output $\log g$ values for a small number of stars is either overestimated or underestimated when compared to isochrone predictions. Some weak trends are also present across the results for the full sample in Fig. 9, with thin columns of stars with very similar effective temperatures but different metallicity values. We do not know exactly what causes these trends. We find these values to cluster around multiples of 100 K, and *MARCS* models have spacings of 100 K for $2500 \text{ K} < T_{\text{eff}} < 4000 \text{ K}$ (compared with 250 K for $4000 \text{ K} < T_{\text{eff}} < 8000 \text{ K}$), but further tests with the interpolation of the models have not shown any issues.

The lower limit of our analysis is around $T_{\text{eff}} = 3000$ K. From the sample of stars with ASPCAP $T_{\text{eff}} < 3000$ K, we found

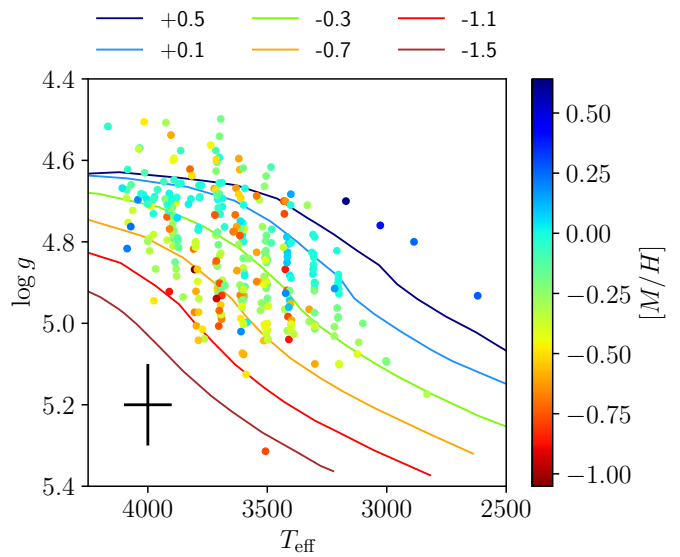


Fig. 8. HR diagram with T_{eff} and $\log g$ values from iSpec output parameter distribution, with overplotted PARSEC isochrones (Bressan et al. 2012) for an age of 5Gyr created with different $[M/H]$ values (scale is in dex). Points are color-coded based on the metallicity value derived for each star. Plotted parameters were obtained with APOGEE DR16

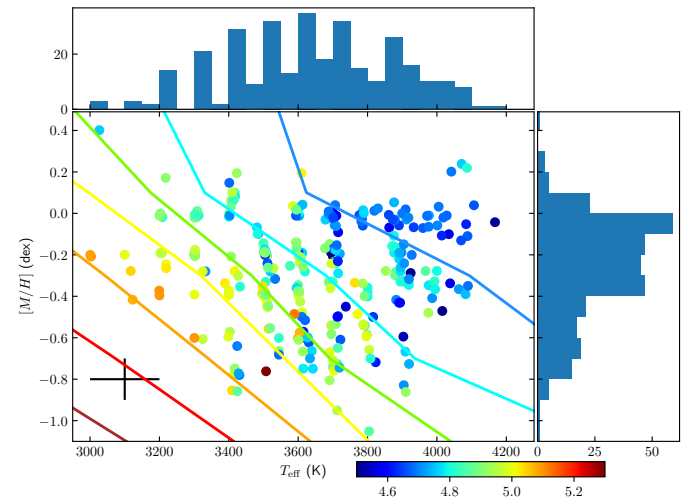


Fig. 9. T_{eff} and $[M/H]$ from iSpec parameter distribution for stars in M dwarf sample, with overplotted PARSEC isochrones (Bressan et al. 2012) for an age of 5Gyr created with different $\log g$ values (scale is in dex). Points are color-coded based on the surface gravity value derived for each star. Plotted parameters were obtained with APOGEE DR16

the normalization template with the lowest χ^2 for 3 of them to converge to synthetic spectra with very high metallicity values ($[M/H] = 0.4$ dex) (see Table 3 for the full results derived for these stars). This correspond to the highest possible $[M/H]$ using our normalization method, and to the limit of the *MARCS* models used to generate synthetic spectra. The output parameters for these three stars are very similar between them, and are outside the expected values for M dwarfs. We do not think these output parameters represent a reliable measurement for these stars, and they are included here only as a demonstration of the limitations of our method for stars with $T_{\text{eff}} < 3000$ K. We think that our pipeline's limitations are caused by our optimization of the line list to reproduce the spectra of stars with higher T_{eff} , missing

Table 1. Average and standard deviation for stellar parameters measured for a sample of 4 stars, using different normalization templates and across 20 iterations of the pipeline for each star/normalization template combination. All displayed T_{eff} values are in K, while $\log g$ and $[M/H]$ are in dex.

Star	Normalization			iSpec Output			
	T_{eff}	$\log g$	$[M/H]$	T_{eff}	$\log g$	$[M/H]$	χ^2
2M00243855+5119224	3700	4.9	-0.6	3681 ± 3	5.16 ± 0.02	-0.49 ± 0.01	0.0455 ± 0.0007
2M00243855+5119224	3700	4.9	-0.8	3671 ± 2	5.12 ± 0.02	-0.55 ± 0.02	0.0464 ± 0.0006
2M00243855+5119224	3700	5	-0.8	3674 ± 4	5.14 ± 0.02	-0.54 ± 0.02	0.0462 ± 0.0008
2M01195227+8409327	3100	5	-0.2	3113 ± 7	4.99 ± 0.01	-0.22 ± 0.03	0.196 ± 0.002
2M01195227+8409327	3100	5.1	-0.2	3134 ± 10	5.07 ± 0.01	-0.29 ± 0.04	0.198 ± 0.003
2M01195227+8409327	3200	5	-0.2	3201 ± 4	5.05 ± 0.04	-0.22 ± 0.02	0.201 ± 0.003
2M01195227+8409327	3200	5.1	-0.4	3202 ± 1	5.13 ± 0.01	-0.38 ± 0.01	0.199 ± 0.003
2M03431519+5006558	3300	4.8	0	3296 ± 1	4.93 ± 0.01	0.03 ± 0.01	0.191 ± 0.002
2M03431519+5006558	3300	4.9	0	3301 ± 1	4.94 ± 0.01	0.03 ± 0.01	0.190 ± 0.002
2M03431519+5006558	3300	5	-0.2	3275 ± 10	4.88 ± 0.04	-0.06 ± 0.05	0.204 ± 0.004
2M03431519+5006558	3400	4.9	-0.2	3352 ± 10	5.02 ± 0.03	-0.05 ± 0.03	0.188 ± 0.003
2M23460112+7456172	3600	5.1	-0.8	3578 ± 4	5.20 ± 0.01	-0.55 ± 0.03	0.069 ± 0.001
2M23460112+7456172	3700	5	-0.8	3678 ± 4	5.20 ± 0.01	-0.64 ± 0.03	0.072 ± 0.001
2M23460112+7456172	3700	5.1	-1	3675 ± 4	5.20 ± 0.01	-0.7 ± 0.03	0.072 ± 0.001
2M23460112+7456172	3800	4.9	-0.6	3770 ± 2	5.10 ± 0.01	-0.68 ± 0.02	0.080 ± 0.001
2M23460112+7456172	3900	4.9	-0.8	3845 ± 3	5.10 ± 0.01	-0.82 ± 0.02	0.088 ± 0.001

Table 2. Average and standard deviation for stellar parameters measured for multiple iterations for 20 selected stars representative of the full sample. 20 iterations were made for each of 16 test stars, while the code was made to run 100 iterations for 4 selected stars. All displayed T_{eff} values are in K, while $\log g$ and $[M/H]$ are in dex. The “Runs” column displays the number of iterations made with the pipeline for each spectrum.

Star	T_{eff}	$\log g$	$[M/H]$	S/N	Runs
2M00391896+5508132	3329 ± 5	5.05 ± 0.02	-0.72 ± 0.04	767	20
2M02465257+5619505	3506 ± 6	4.69 ± 0.02	-0.29 ± 0.02	346	20
2M04244284+4537062	3859 ± 4	4.68 ± 0.03	-0.44 ± 0.01	257	20
2M04422854+5818015	3312 ± 5	5.05 ± 0.01	-0.26 ± 0.03	615	20
2M05201152+2457212	3667 ± 7	4.59 ± 0.03	-0.06 ± 0.03	677	20
2M06070493+1403109	3292 ± 3	5.08 ± 0.02	-0.21 ± 0.01	258	20
2M06572462+0651440	3307 ± 8	5.03 ± 0.03	-0.24 ± 0.04	197	20
2M08050361+4121251	3340 ± 7	4.91 ± 0.03	-0.68 ± 0.06	222	20
2M10562960+4858264	4063 ± 12	4.76 ± 0.02	0.21 ± 0.01	328	20
2M11152550+0003159	3424 ± 4	4.87 ± 0.03	-0.77 ± 0.04	294	20
2M13552585+2556161	4013 ± 4	4.51 ± 0.01	-0.48 ± 0.01	177	20
2M14535251+1739448	3801 ± 3	4.67 ± 0.02	-0.51 ± 0.01	619	20
2M16495034+4745402	3754 ± 6	4.69 ± 0.02	-0.01 ± 0.01	1147	20
2M18055545+0316213	3573 ± 2	4.63 ± 0.01	0 ± 0.01	229	20
2M19004176+0310312	3512 ± 6	4.95 ± 0.03	-0.77 ± 0.09	170	20
2M23134861+1227072	3560 ± 2	5 ± 0.01	0 ± 0.01	172	20
2M03190939+0130543	2972 ± 3	4.7 ± 0.02	0.22 ± 0.01	161	100
2M04552111+5017249	3882 ± 3	4.66 ± 0.03	-0.87 ± 0.02	177	100
2M09301445+2630250	3385 ± 2	4.67 ± 0.02	0.14 ± 0.01	658	100
2M21400112+5408179	3592 ± 3	5.03 ± 0.02	-0.55 ± 0.02	563	100

possible opacity sources for lower temperature stars, and the pipeline compensating these deficiencies by decreasing the T_{eff} and increasing the $[M/H]$ of the synthetic spectra. These effects increase the strength of the water lines present in the spectrum, but the resulting parameters will not be reliable.

We find the spectra of stars with $3000 < T_{\text{eff}} < 3500$ K to be especially challenging to synthetically reproduce due to the degeneracy in continuum absorption between multiple spectral parameters such as temperature, metallicity, and surface gravity. Absorptions in the continuum can be caused by any of these parameters, with the pipeline sometimes estimating lower metallicity and higher temperature values than the star has in reality.

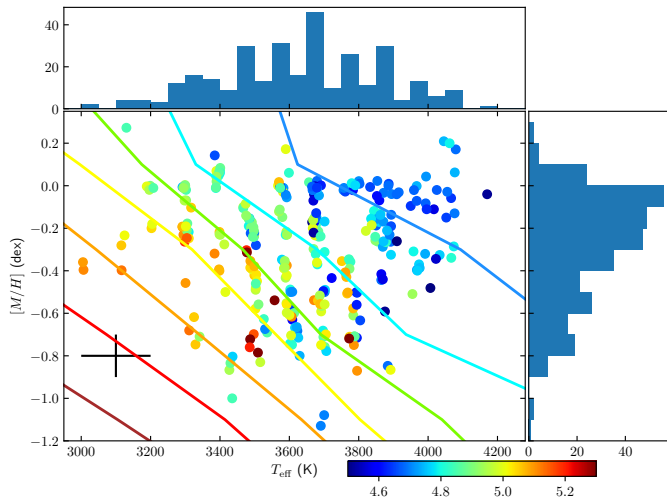
We present an example synthesized stellar spectra for a star with $T_{\text{eff}} \sim 3500$ K in Fig. 11. Here, the spectra of star

2M18244689-0620311 (BD-06 4756B²) is displayed, showing both the observed (black) and best matching spectra (red). This star was characterized in Souto et al. (2020) as having $T_{\text{eff}} = 3376$ K, $\log g = 4.77$ dex, $[M/H] = +0.21$ dex. The available AS-PCAP parameters for this star are $T_{\text{eff}} = 3502$ K, $\log g = 4.63$ dex, and $[M/H] = -0.17$ dex. The displayed spectrum for the star has been obtained by normalizing the APOGEE observed one with a synthetic spectrum with $T_{\text{eff}} = 3500$ K, $\log g = 4.9$ dex and $[M/H] = -0.2$ dex, and the derived spectroscopical parameters for this star are $T_{\text{eff}} = 3484 \pm 100$ K, $\log g = 4.85 \pm 0.2$ dex, $[M/H] = -0.15 \pm 0.1$ dex.

² <http://simbad.u-strasbg.fr/simbad/sim-id?Ident=2Mass+j18244689-0620311>

Table 3. Output parameters for 6 stars with $T_{\text{eff}} \leq 3000$ K. All T_{eff} values are in Kelvin, [M/H] in dex and $\log g$ in dex.

Star	iSpec Output			Normalization		
	T_{eff}	$\log g$	[M/H]	T_{eff}	$\log g$	[M/H]
2M02081366+4949023	2886	4.80	0.25	2900	5.0	0.4
2M05392474+4038437	2619	4.93	0.28	2600	5.1	0.4
2M06481555+0326243	2831	5.17	-0.31	2800	5.2	-0.2
2M13481341+2336486	3003	5.09	-0.21	3000	5.1	-0.2
2M14562713+1755001	3117	5.05	-0.28	3100	5.0	-0.2
2M20032651+2952000	3027	4.76	0.40	3000	4.9	0.4

**Fig. 10.** T_{eff} and [M/H] from iSpec parameter distribution for stars in M dwarf sample, with overplotted PARSEC isochrones (Bressan et al. 2012) for an age of 5Gyr created with different $\log g$ values (scale is in dex). Points are color-coded based on the surface gravity value derived for each star. Plotted parameters were obtained with APOGEE DR14

The presence of a wide water line band is noticeable across the full spectrum, especially the full first order (two top rows), resulting in a jagged and depressed continuum down to around 0.9 instead of the expected 1.0. The modeling of these water lines is fundamental for the creation of an accurate synthetic spectra of late M dwarfs ($T_{\text{eff}} < 3500$ K). This star is slightly below solar metallicity, still having pronounced molecular and elemental lines. The effect can be noticed in the strong Al line around 1675 nm, a line accurately matched by the synthetic spectrum. The synthesized spectrum matches the observed one across the full wavelength range, with lines of multiple elements and molecules being correctly synthesized. This fact, combined with the relative agreement of our pipeline's derived parameter with available literature analysis, increases our confidence in the derived parameters for this star.

Additional examples of output spectra obtained by our pipeline are displayed in the appendix, in Figs. B.2 to B.5, with more stars across our parameter space.

5. Analysis

5.1. ASPCAP comparison

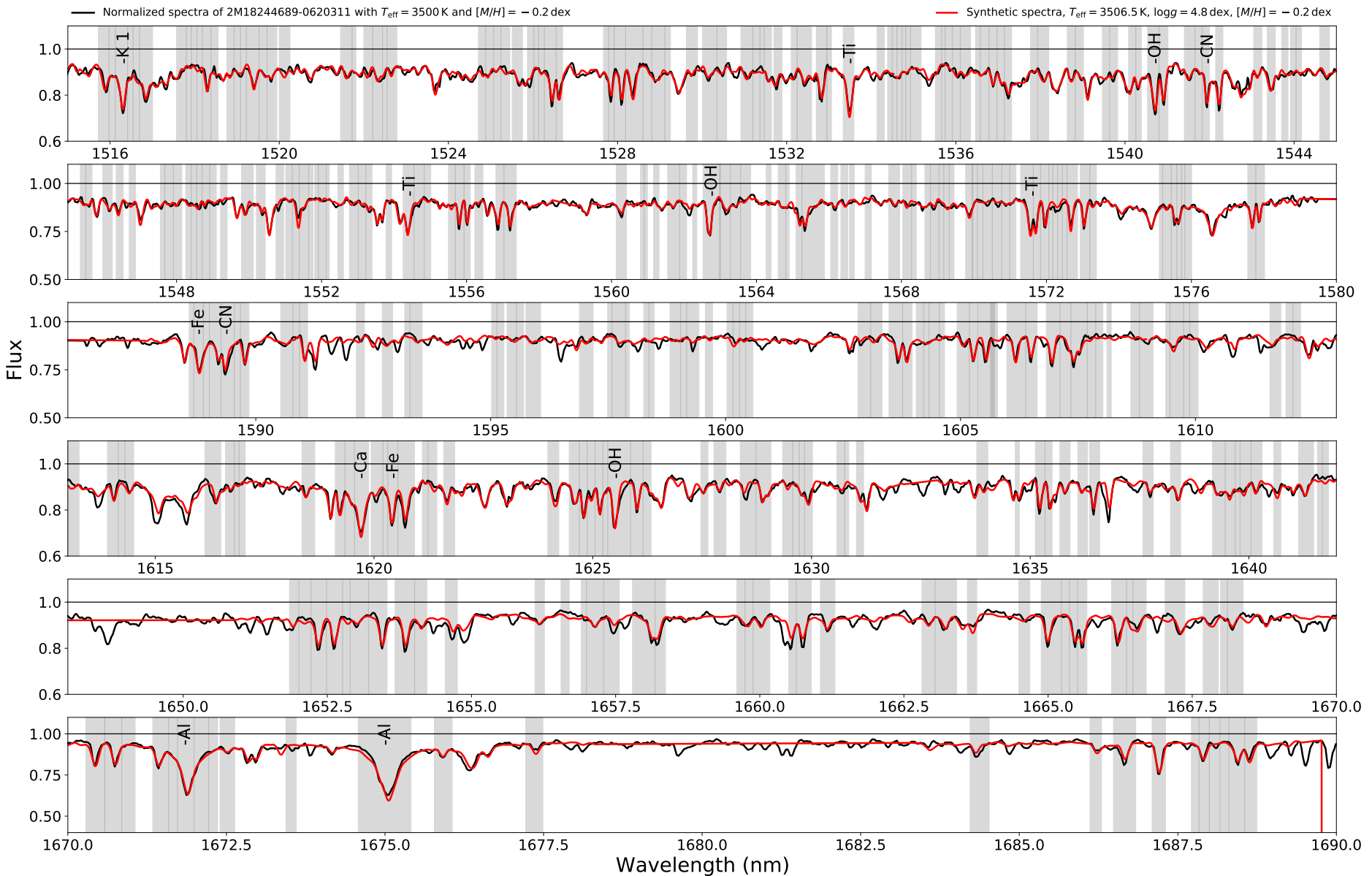


Fig. 11. Comparison between APOGEE spectra of the star 2M18244689-0620311 (black, normalized using a synthetic spectra with $T_{\text{eff}} = 3500$ K, $\log g = 4.9$ dex and $[M/H] = -0.2$ dex) and the best fitting synthetic spectra (red, straight line) for APOGEE wavelength range. In gray highlight are the areas used for χ^2 minimization by our pipeline's algorithm. The best fitting parameters derived were $T_{\text{eff}} = 3507 \pm 100$ K, $\log g = 4.80 \pm 0.2$ dex, $[M/H] = -0.19 \pm 0.1$ dex. The available ASPCAP parameters are $T_{\text{eff}} = 3600 \pm 59$ K, $\log g = 5.09 \pm 0.12$ dex and $[M/H] = -0.06 \pm 0.01$ dex. This star was characterized in Souto et al. (2020) as having $T_{\text{eff}} = 3376$ K, $\log g = 4.77$ dex, $[M/H] = +0.21$ dex.

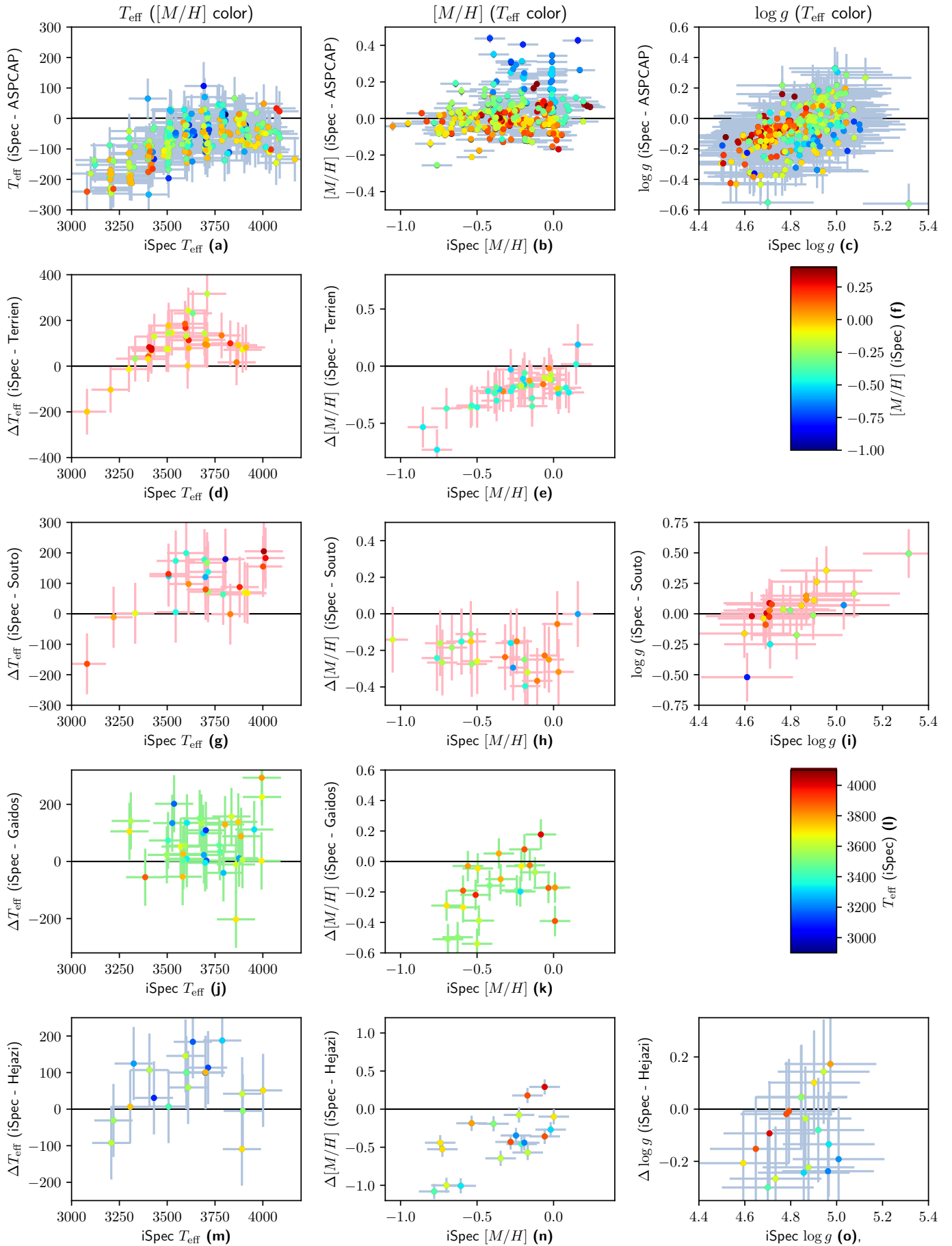


Fig. 12. Comparisons between our output parameters and ones available in literature, colored accordingly to either our method's measured $[M/H]$ (T_{eff} plots, left column, see scale at (f)) or T_{eff} for each star ($[M/H]$, center column, and $\log g$, right column, see color scale at (l)). From the top to bottom: comparisons with ASPCAP (a, b, c), Terrien et al. (2015) (d, e), Souto et al. (2020) (g, h, i), Gaidos et al. (2014) (m, n, o), Hejazi et al. (2019) (j, k). Temperature values are displayed in Kelvin, while metallicity and surface gravity are in dex.

Table 4. Median differences between our results and literature parameters. All displayed ASPCAP parameters (T_{eff} , $[M/H]$ and $\log g$) are from their calibrated values. Median difference is calculated by subtracting literature parameters from our results. SD stands for standard deviation and MAD for Median Absolute Deviation. Temperature values are displayed in Kelvin, while metallicity and surface gravity are in dex.

Parameter	Stars	Median	SD	MAD
ASPCAP				
T_{eff}	283	-63	70	58
$[M/H]$	283	+0.0	0.15	0.08
$\log g$	283	-0.07	0.14	0.11
Terrien et al. (2015)				
T_{eff}	45	+92	86	57
$[M/H]$	45	-0.19	0.15	0.08
Souto et al. (2020)				
T_{eff}	24	+109	85	77
$[M/H]$	24	-0.23	0.09	0.11
$\log g$	24	+0.03	0.20	0.11
Gaidos et al. (2014)				
T_{eff}	40	+56	91	81
$[M/H]$	24	-0.17	0.19	0.19
Hejazi et al. (2019)				
T_{eff}	19	+59	81	78
$[M/H]$	19	-0.43	0.36	0.32
$\log g$	19	-0.09	0.14	0.19

As mentioned in Section 2.3, there are no available final ASPCAP spectroscopic parameters for all stars in our sample. From the full 313 star sample, we have ASPCAP calibrated values for T_{eff} , $[M/H]$, and $\log g$ for 283 of them. Therefore, all comparisons shown and discussed here will focus on those 283 stars. We do not show raw/spectroscopic parameters for consistency reasons. Fig. 12 (a) shows a comparison between the T_{eff} values for our sample M dwarfs as derived by our pipeline and the calibrated values published by ASPCAP for the same stars, (b) presents the same comparison for ASPCAP calibrated $[M/H]$ values, and (c) shows a comparison between the $\log g$ values derived with our pipeline and the calibrated ones published by ASPCAP. Errors included are estimated based on our normalization grids and are ± 100 K for the T_{eff} , ± 0.1 dex for $[M/H]$ and ± 0.2 dex for $\log g$ (see section 3.5). The points are colored accordingly to other parameters measured by our method in order to highlight any correlation or trend between errors across multiple output parameters.

In Fig. 12 (a), and relative to ΔT_{eff} , we find a small trend of more negative ΔT_{eff} for stars with $T_{\text{eff}} < 3500$ K. For stars above this T_{eff} , we find very similar values between our analysis and the parameters published by ASPCAP. Additionally, we find no correlation between ΔT_{eff} and each star's metallicity values. Overall, we find this parameter to have a good agreement with ASPCAP published results, with the median difference, SD and MAD all being within our error margins.

As for Fig. 12 (b) and $[M/H]$, a trend is present here, as we find a negative $\Delta[M/H]$ for the stars in our sample with $T_{\text{eff}} > 3400$ K and a positive one for stars with $T_{\text{eff}} < 3400$ K. This translates to an overestimation of metallicity for the colder stars in our sample, when compared to ASPCAP values. Both lower T_{eff} and increasing $[M/H]$ can have a similar effect on the spectral shape, lowering the continuum position due to an increased strength of the water molecular lines. Therefore, metallicity overestimations can be caused by normalization errors and/or correspond to effective temperature underestimations. We have to

note that we are using the T_{eff} values determined by our pipeline to color the points.

For $\log g$, Fig. 12 (c) shows that a small trend is present in the data, with negative $\Delta \log g$ values for stars with lower $\log g$. The overall distribution is not very different, with median differences of +0.07 dex between our parameters and the ones published by ASPCAP, although with SD and MAD around our uncertainty levels. We find a wide range of differences in $\log g$, with the comparisons varying between -0.6 dex and +0.4 dex. Comparisons with the isochrones in Fig. 8 show that our values for this parameter are within the expectations for main-sequence stars around these temperatures. A direct comparison between Figs. 3, 9 and 10 shows how the ASPCAP calibrated $\log g$ values differ from our derived parameters for our M dwarf sample. While our values using data from DR16 follow the isochrones approximately, both the results with DR14 and their parameters seem to vary wildly, especially for M dwarfs with $T_{\text{eff}} < 3800$ K / $\log g > 4.9$ dex. This does seem to indicate that our method provides more plausible surface gravity values, given our current stellar modeling knowledge reflected in the overplotted PARSEC isochrones. It also shows how the spectra provided by APOGEE improved between DR14 and DR16, lending credence to the more recent Data Release as being of higher quality than the previous one.

Overall, we find that the best agreement between our parameters and the ones published by ASPCAP is found for $[M/H]$, despite some trends being present alongside T_{eff} and $\log g$. All of these comparisons are made with calibrated ASPCAP parameters. These should not be ignored, as they can show inherent bias in the method and the output parameters.

5.2. Other literature comparisons

5.2.1. Comparison with Terrien et al. (2015)

Fig. 12 (d) and (e) show a comparison between the parameters derived with our pipeline and the ones published in Terrien et al. (2015) for 45 stars in common between both samples. Table 4 shows the median difference, standard deviation and mean absolute deviation found when comparing both distributions. As Terrien et al. (2015) does not publish values for $\log g$, we kept the space reserved for the plot for that parameter (right column) empty. We find the differences between them to be above the uncertainty level, with the SD and MAD of the $[M/H]$ values being slightly above (0.15 and 0.08 dex vs 0.10 dex) and T_{eff} slightly below (86 K and 57 K vs 100 K).

In the case of T_{eff} , we find no large-scale trend or deviation between both parameter distributions, with $\Delta T_{\text{eff}} < 250$ K for all compared stars and with no correlation with $[M/H]$. However, the fact that we find $\Delta T_{\text{eff}} \geq 0$ K for almost the full sample, as well as a median difference of +92 K, points towards small biases in either parameter distribution. As for $\Delta[M/H]$, it has a wider distribution, going up to ± 0.3 dex, and a median difference of -0.19 dex can point towards systematic trends in our output data. There is also a linear trend towards negative $\Delta[M/H]$ for stars with $[M/H] < -0.2$ dex and $T_{\text{eff}} \sim 3300$ K.

5.2.2. Comparison with Souto's parameters

Figs. 12 (g), (h), and (i) show a comparison between the parameters derived by our pipeline and the ones published in Souto et al. (2017); Souto et al. (2018); Souto et al. (2020) for 24 M dwarfs. We should note that, as Souto et al. published $[Fe/H]$ for their characterized stars and our method measures $[M/H]$, that discrepancy can explain some of the differences. The differences

between results published by both methods are also summarized in Table 4.

We find clear differences between both parameter distributions, with lower metallicity values ($\Delta[M/H] = -0.23$ dex) and higher temperatures ($\Delta T_{\text{eff}} = +109$ K) for our stars. These trends fall in line with the results for the previously compared Terrien et al. (2015) results, with negative $\Delta[M/H]$ and positive ΔT_{eff} , with the metallicity differences being above our uncertainty levels. Like the previous comparison, we find no cross-parameter trends, as the $[M/H]$ differences seem to be independent of T_{eff} and vice versa.

We also find a weak linear trend with $\log g$ itself, as we find lower $\Delta \log g$ for stars with $\log g < 4.8$ dex, and a higher $\Delta \log g$ for stars with $\log g > 4.8$ dex (with a correlation coefficient of $\rho = 0.71$).

5.2.3. Comparison with Gaidos et al. (2014)

We present, in Fig. 12 (j), a comparison between our T_{eff} results and the ones published in Gaidos et al. (2014) for 40 stars in common between both samples. Fig. 12 (k) shows a similar comparison for $[M/H]$ for the 24 stars with that parameter in the common sample. Similar to the case of Terrien et al. (2015), we have no reference value for $\log g$ from this source, so the space for the plot for that parameter (right column) is kept empty. Additionally, Table 4 presents the median, standard deviation and mean absolute deviation found when comparing both parameter distributions.

Similar to the previous comparisons, we find trends towards both positive ΔT_{eff} and negative $\Delta[M/H]$. We find the standard (91 K) and mean absolute deviations (81 K) to be slightly around our estimated uncertainties for temperature, while the median differences (+56 K) are below them. As for metallicity, they are slightly above our uncertainty levels. There is a small trend towards lower $\Delta[M/H]$ for colder objects, but since the number of stars is so small it might be just a statistical artifact.

5.2.4. Comparison with Hejazi et al. (2019)

We present, in Figs. 12 (m), (n) and (o), a comparison between our output values and the ones published in Hejazi et al. (2019) for 19 stars in common between both samples. Additionally, Table 4 presents the differences between results obtained by both methods. We find positive ΔT_{eff} , with standard (81 K) and mean absolute (78 K) deviations around our estimated uncertainties for the parameter. We also find strong trends in both $\log g$ and $[M/H]$ distributions, with deviations significantly above our estimated uncertainty values.

As for discrepancies in T_{eff} , Fig. 12 (m) shows that the ΔT_{eff} distribution between both methods is not very large, with most stars having a $\Delta T_{\text{eff}} \sim \pm 120$ K. The strongest outlier is star 2M07404603+3758253, which we find to have $T_{\text{eff}} = 3325$ K and $[M/H] = -0.62$ dex, while Hejazi et al. (2019) published $T_{\text{eff}} = 3200$ K and $[M/H] = +0.4$ dex for the same star³.

A $[M/H]$ comparison shows a linear trend in Fig. 12 (n), with $\Delta[M/H] \sim -1.0$ dex for metal-poor stars, and $\Delta[M/H] \sim 0.0$ dex for stars around solar metallicity. We also find significantly lower values for metallicity than Hejazi et al. (2019), with an average $\Delta[M/H] = -0.43$ dex. Despite their reported uncertainties of ± 0.22 dex, this is a significant difference. Similar to the comparison with Gaidos et al. (2014) (Fig. 12 (k)) and unlike the ASPCAP

comparison (Fig. 12 (b)), there is a trend towards lower $\Delta[M/H]$ for colder objects. Some possible explanations can be the lower resolution of their analysis and the fact that it was done in the optical and not in the near-infrared, but the fact that the trends are very similar across all literature comparisons presented here lead us to believe in the presence of an inherent bias in our pipeline towards low $[M/H]$ output parameters.

For $\log g$, we find a linear trend towards measuring lower $\Delta \log g$ for stars with $\log g < 4.9$ dex, and a higher $\Delta \log g$ for stars with $\log g > 4.9$ dex. This is very similar to the $\Delta \log g$ plot for our Souto values comparison (see Fig. 12 (i)) and can point towards some issues with the $\log g$ determined by our method.

5.2.5. Comparison with Rajpurohit et al. (2018b)

We display a comparison between our output parameters and the results published by Rajpurohit et al. (2018b) for 8 stars in common in Fig. 13. Due to the low number of stars compared, no real statistical analysis can be made from this comparison. We find some small differences in the results across the stellar sample, with the clearest example being star 2M06320207+3431132, with an output $T_{\text{eff}} = 3465$ K (our results) vs 3200 K. Similar to the previous comparisons, we find an overall positive, but close to our uncertainty levels, ΔT_{eff} . Unlike the previous results, we actually find a positive $\Delta[M/H]$ as well, while the largest difference between our results and theirs is in surface gravity, with some stars having $\Delta \log g \sim -0.6$ dex.

5.2.6. Comparison with Rajpurohit et al. (2018a) and Passegger et al. (2019)

As our sample and both Rajpurohit et al. (2018a) and Passegger et al. (2019)'s have only 12 stars and 14 stars in common, respectively, we compared our results with the parameters for each of them in Fig. 13. No overall trends are present in T_{eff} , with the exception of a single star, 2M11474440+0048164, that has Rajpurohit et al. (2018a) $T_{\text{eff}} = 3500$ K and our analysis output is $T_{\text{eff}} = 3202$ K. This star, however is characterized in Passegger et al. (2019) as having $T_{\text{eff}} = 3267$ K, and by Souto et al. (2018) as having $T_{\text{eff}} = 3231$ K. Both these literature values are much closer to our results, explaining the results of Rajpurohit et al. (2018a) as an outlier. As for metallicity, we find $\Delta[M/H] \sim -0.3$ dex, in line with other literature comparisons, and keep in mind that the comparison with Passegger et al. (2019) is based on their values for $[Fe/H]$ rather than $[M/H]$. As for $\log g$, we find our output parameters to be very similar to the ones published by Passegger et al. (2019), but some differences are present in the comparison with Rajpurohit et al. (2018a), with our values being up to 0.8 dex below theirs for 3 stars in common. However, similarly to the T_{eff} for star 2M11474440+0048164, the $\log g$ values published by Passegger et al. (2019) for these stars are also much closer to our measurements, with a $\Delta \log g \sim 0.05$ dex.

6. Conclusions

Building on the method previously presented in Sarmento et al. (2020), we derived stellar atmospheric parameters for 313 M dwarfs with $3000 \text{ K} < T_{\text{eff}} \pm 100 \text{ K} < 4200 \text{ K}$, $4.5 \text{ dex} < \log g \pm 0.2 \text{ dex} < 5.3 \text{ dex}$ and $-1.05 \text{ dex} < [M/H] \pm 0.1 \text{ dex} < 0.56 \text{ dex}$. The pipeline uses *iSpec* as a spectroscopic framework to control *Turbospectrum* code, and requires both a complete line list at the studied wavelength and a line mask tailored for the spectral type of the analyzed stars. We include both of these resources with

³ A plot comparing our best synthetic fit to the observed APOGEE spectra is included in the Appendix as Fig. B.6.

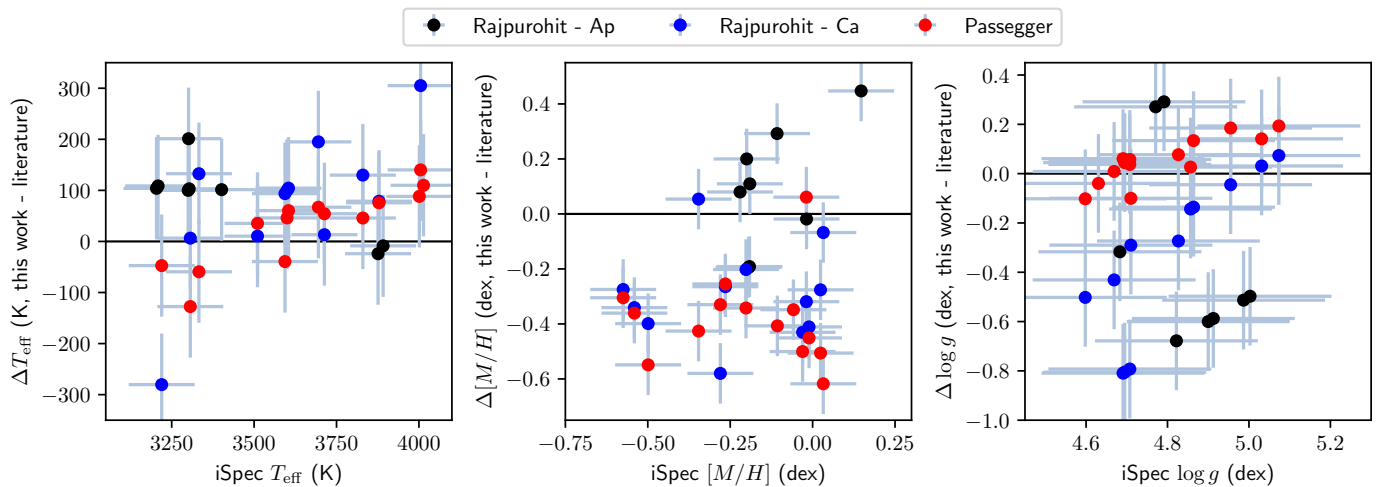


Fig. 13. Comparison in derived parameters between our method and the eight stars in common with Rajpurohit et al. (2018b) (APOGEE) and the twelve stars in common with Rajpurohit et al. (2018a) (CARMENES), and fourteen with Passegger et al. (2019) (our pipeline - literature).

the paper, as well as all the derived stellar parameters, for future reference.

A series of literature comparisons demonstrates the difficulty of finding accurate parameters for M dwarfs. Positive ΔT_{eff} values are found across multiple literature comparisons, except for the ASPCAP values, although usually within uncertainty levels. However, the additional presence of negative $\Delta[M/H]$ values in most of our literature comparisons suggest the existence of issues with the temperature and metallicity determination in our pipeline, as the effects of changes in these parameters in the M dwarf regime are not independent. We also note that our results are also dependent on the assumptions of the PARSEC evolutionary code. More analysis needs to be done on this subject.

Despite the existence of these trends, the strong matching between synthesized and observed spectra for a wide range of M dwarf stars shows the power of the pipeline as a method for parameter determination. Future works could apply the method to Near-Infrared spectra observed with other instruments with better resolution than APOGEE, such as CARMENES ($R = 80\,000 - 100\,000$, Quirrenbach et al. 2014), GIANO ($R \sim 50\,000$, Origlia et al. 2014), SPIROU ($R \sim 75\,000$, Artigau et al. 2014), NIRPS ($R \sim 90\,000 - 100\,000$ Wildi et al. 2017), and CRIRES+ ($R \sim 100\,000$, Dorn et al. 2014). Expanding the characterized parameter space, through an analysis of a larger M dwarf sample, together with an expansion to more complete and detailed molecular line lists, are other possibilities to improve the performance of our method.

Acknowledgements. This work was supported by FCT - Fundação para a Ciência e a Tecnologia through national funds (PTDC/FIS-AST/28953/2017, PTDC/FIS-AST/7073/2014, PTDC/FIS-AST/32113/2017, UID/FIS/04434/2013) and by FEDER - Fundo Europeu de Desenvolvimento Regional through COMPETE2020 - Programa Operacional Competitividade e Internacionalização (POCI-01-0145-FEDER-028953, POCI-01-0145-FEDER-016880, POCI-01-0145-FEDER-032113, POCI-01-0145-FEDER-007672). This work was supported by Fundação para a Ciência e a Tecnologia (FCT) through the research grants UID/FIS/04434/2019, UIDB/04434/2020 and UIDP/04434/2020. This research has made use of NASA's Astrophysics Data System. P.S. acknowledges the support by the Bolsa de Investigação PD/BD/128050/2016. E.D.M. acknowledges the support by the Investigador FCT contract IF/00849/2015/CP1273/CT0003 and in the form of an exploratory project with the same reference. B.R.-A acknowledges funding support from FONDECYT through grant 11181295.

References

- Ahumada, R., Allende Prieto, C., Almeida, A., et al. 2019, arXiv e-prints, arXiv:1912.02905
- Ahumada, R., Prieto, C. A., Almeida, A., et al. 2020, ApJS, 249, 3
- Alonso-Floriano, F., Morales, J., Caballero, J., et al. 2015, Astronomy & Astrophysics, 577, A128
- Alvarez, R. & Plez, B. 1998, 330, 1109
- Artigau, É., Kouach, D., Donati, J.-F., et al. 2014, in Ground-based and Airborne Instrumentation for Astronomy V, Vol. 9147, International Society for Optics and Photonics, 914715
- Barber, R., Tennyson, J., Harris, G. J., & Tolchenov, R. 2006, Monthly Notices of the Royal Astronomical Society, 368, 1087
- Blanco-Cuaresma, S. 2019, mnras, 486, 2075
- Blanco-Cuaresma, S., Soubiran, C., Heiter, U., & Jofré, P. 2014, Astronomy & Astrophysics, 569, A111
- Bochanski, J. J., Munn, J. A., Hawley, S. L., et al. 2007, The Astronomical Journal, 134, 2418
- Bonfils, X., Delfosse, X., Udry, S., et al. 2013, Astronomy & Astrophysics, 549, A109
- Bowen, I. & Vaughan, A. 1973, Applied Optics, 12, 1430
- Boyajian, T. S., von Braun, K., van Belle, G., et al. 2013, apj, 771, 40
- Bressan, A., Marigo, P., Girardi, L., et al. 2012, Monthly Notices of the Royal Astronomical Society, 427, 127
- Casagrande, L., Flynn, C., & Bessell, M. 2008, Monthly Notices of the Royal Astronomical Society, 389, 585
- Delfosse, X., Forveille, T., Ségransan, D., et al. 2000, arXiv preprint astro-ph/0010586
- Deshpande, R., Blake, C., Bender, C., et al. 2013, The Astronomical Journal, 146, 156
- Dorn, R. J., Anglada-Escude, G., Baade, D. a., et al. 2014, The Messenger, 156
- France, K., Froning, C. S., Linsky, J. L., et al. 2013, The Astrophysical Journal, 763, 149
- Gaidos, E., Mann, A., Lépine, S., et al. 2014, Monthly Notices of the Royal Astronomical Society, 443, 2561
- Garcia Pérez, A. E., Prieto, C. A., Holtzman, J. A., et al. 2016, The Astronomical Journal, 151, 144
- Gunn, J. E., Siegmund, W. A., Mannery, E. J., et al. 2006, The Astronomical Journal, 131, 2332
- Gustafsson, B., Edvardsson, B., Eriksson, K., et al. 2008, aap, 486, 951
- Hejazi, N., Lepine, S., Homeier, D., Rich, R. M., & Shara, M. M. 2019, arXiv e-prints, arXiv:1911.04612
- Henry, T. J., Jao, W.-C., Subasavage, J. P., et al. 2006, The Astronomical Journal, 132, 2360
- Holmberg, J., Nordström, B., & Andersen, J. 2007, Astronomy & Astrophysics, 475, 519
- Holtzman, J. A., Hasselquist, S., Shetrone, M., et al. 2018, The Astronomical Journal, 156, 125
- Irwin, J. M., Berta-Thompson, Z. K., Charbonneau, D., et al. 2014, arXiv preprint arXiv:1409.0891
- Jönsson, H., Holtzman, J. A., Allende Prieto, C., et al. 2020, AJ, 160, 120
- Latham, D., Brown, T., Monet, D., et al. 2005, in Bulletin of the American Astronomical Society, Vol. 37, 1340

- Lépine, S. & Gaidos, E. 2011, *The Astronomical Journal*, 142, 138
 Lépine, S., Rich, R. M., & Shara, M. M. 2007, *The Astrophysical Journal*, 669, 1235
 Lépine, S. & Shara, M. M. 2005, *The Astronomical Journal*, 129, 1483
 López-Valdivia, R., Mace, G. N., Sokal, K. R., et al. 2019, arXiv preprint arXiv:1905.05076
 Majewski, S. R., Schiavon, R. P., Frinchaboy, P. M., et al. 2017, *The Astronomical Journal*, 154, 94
 Mann, A. W., Brewer, J. M., Gaidos, E., Lépine, S., & Hilton, E. J. 2013, *The Astronomical Journal*, 145, 52
 Mann, A. W., Feiden, G. A., Gaidos, E., Boyajian, T., & von Braun, K. 2015, *The Astrophysical Journal*, 804, 64
 Markwardt, C. B. 2009, arXiv preprint arXiv:0902.2850
 Ness, M., Hogg, D. W., Rix, H.-W., et al. 2016, *The Astrophysical Journal*, 823, 114
 Önehag, A., Heiter, U., Gustafsson, B., et al. 2012, *Astronomy & Astrophysics*, 542, A33
 Origlia, L., Oliva, E., Baffa, C., et al. 2014, in *Ground-based and Airborne Instrumentation for Astronomy V*, Vol. 9147, International Society for Optics and Photonics, 91471E
 Passegger, V., Schweitzer, A., Shulyak, D., et al. 2019, *Astronomy & Astrophysics*, 627, A161
 Piskunov, N., Kupka, F., Ryabchikova, T., Weiss, W., & Jeffery, C. 1995, *Astronomy and Astrophysics Supplement Series*, 112, 525
 Plez, B. 2012, *Astrophysics Source Code Library*, 1, 05004
 Polyansky, O. L., Kyuberis, A. A., Zobov, N. F., et al. 2018, *Monthly Notices of the Royal Astronomical Society*, 480, 2597
 Quirrenbach, A., Amado, P., Caballero, J., et al. 2014, in *Ground-based and airborne instrumentation for astronomy V*, Vol. 9147, International Society for Optics and Photonics, 91471F
 Rajpurohit, A., Allard, F., Rajpurohit, S., et al. 2018a, *Astronomy & Astrophysics*, 620, A180
 Rajpurohit, A., Allard, F., Teixeira, G., et al. 2018b, *Astronomy & Astrophysics*, 610, A19
 Rojas-Ayala, B., Covey, K. R., Muirhead, P. S., & Lloyd, J. P. 2010, *The Astrophysical Journal Letters*, 720, L113
 Rojas-Ayala, B., Covey, K. R., Muirhead, P. S., & Lloyd, J. P. 2012, *The Astrophysical Journal*, 748, 93
 Santos, N., Sousa, S., Mortier, A., et al. 2013, *Astronomy & Astrophysics*, 556, A150
 Sarmento, P., Mena, E. D., Rojas-Ayala, B., & Blanco-Cuaresma, S. 2020, arXiv preprint arXiv:2001.01995
 Scalo, J., Kaltenegger, L., Segura, A., et al. 2007, *Astrobiology*, 7, 85
 Schmidt, S. J., Wagoner, E. L., Johnson, J. A., et al. 2016, *Monthly Notices of the Royal Astronomical Society*, 460, 2611
 Segura, A., Kasting, J. F., Meadows, V., et al. 2005, *Astrobiology*, 5, 706
 Shetrone, M., Bizyaev, D., Lawler, J. E., et al. 2015, *The Astrophysical Journal Supplement Series*, 221, 24
 Sousa, S. G., Santos, N. C., Israelian, G., et al. 2011, *Astronomy & Astrophysics*, 526, A99
 Souto, D., Cunha, K., García-Hernández, D. A., et al. 2017, 835, 239
 Souto, D., Cunha, K., Smith, V. V., et al. 2020, arXiv e-prints, arXiv:2001.05597
 Souto, D., Unterborn, C. T., Smith, V. V., et al. 2018, *The Astrophysical Journal Letters*, 860, L15
 Suda, T., Katsuta, Y., Yamada, S., et al. 2008, *Publications of the Astronomical Society of Japan*, 60, 1159
 Terrien, R. C., Mahadevan, S., Deshpande, R., & Bender, C. F. 2015, *The Astrophysical Journal Supplement Series*, 220, 16
 Veyette, M. J., Muirhead, P. S., Mann, A. W., et al. 2017, *The Astrophysical Journal*, 851, 26
 Wildi, F., Blind, N., Reshetov, V., et al. 2017, in *Techniques and Instrumentation for Detection of Exoplanets VIII*, Vol. 10400, International Society for Optics and Photonics, 1040018
 Zasowski, G., Johnson, J. A., Frinchaboy, P., et al. 2013, *The Astronomical Journal*, 146, 81

Appendix A: Parameter combination list for the normalization

T_{eff} (K)	$\log g$ (dex)	[M/H] (dex)
2500	-0.4	5.3
2500	0	5.2
2500	0.2	5.1
2500	0.4	5.1
2600	-0.6	5.3
2600	-0.4	5.2
2600	-0.2	5.2
2600	0	5.1
2600	0	5.2
2600	0.2	5.1
2600	0.4	5.1
2600	0.4	5
2700	-0.8	5.3
2700	-0.6	5.3
2700	-0.4	5.2
2700	-0.2	5.2
2700	0	5.1
2700	0.2	5.1
2700	0.4	5
2800	-1	5.3
2800	-1	5.4
2800	-0.8	5.3
2800	-0.6	5.3
2800	-0.2	5.2
2800	0	5.1
2800	0.2	5.1
2800	0.4	5.1
2800	0.4	5
2900	-1	5.3
2900	-0.8	5.3
2900	-0.4	5.2
2900	-0.2	5.1
2900	0	5.1
2900	0.2	5
2900	0.4	5
2900	0.4	4.9
3000	-1	5.3
3000	-0.8	5.2
3000	-0.8	5.3
3000	-0.6	5.2
3000	-0.4	5.1
3000	-0.2	5.1
3000	0	5
3000	0.2	5
3000	0.4	4.9
3100	-1	5.3
3100	-0.8	5.2
3100	-0.6	5.2
3100	-0.4	5.1
3100	-0.2	5.1
3100	-0.2	5
3100	0	5
3100	0.2	4.9
3100	0.4	4.9
3100	0.4	4.8
3200	-1	5.2
3200	-1	5.3
3200	-0.8	5.2
3200	-0.6	5.1

T_{eff} (K)	$\log g$ (dex)	[M/H] (dex)
3200	-0.4	5.1
3200	-0.2	5
3200	0	4.9
3200	0.2	4.9
3200	0.2	4.8
3200	0.4	4.8
3300	-0.8	5.1
3300	-0.6	5.1
3300	-0.4	5
3300	-0.2	4.9
3300	-0.2	5
3300	0	4.9
3300	0	4.8
3300	0.2	4.8
3300	0.4	4.8
3400	-1	5.2
3400	-0.8	5.1
3400	-0.6	5.1
3400	-0.6	5
3400	-0.4	5
3400	-0.4	4.9
3400	0	4.8
3400	0.2	4.8
3400	0.2	4.7
3400	0.4	4.8
3400	0.4	4.7
3500	-1	5.2
3500	-1	5.1
3500	-0.8	5.1
3500	-0.6	5.1
3500	-0.6	5
3500	-0.4	5
3500	-0.4	4.9
3500	-0.2	4.9
3500	-0.2	4.8
3500	0	4.8
3500	0.2	4.7
3500	0.2	4.7
3500	0.4	4.7
3600	-1	5.1
3600	-0.8	5.1
3600	-0.8	5
3600	-0.6	5
3600	-0.6	4.9
3600	-0.4	4.9
3600	-0.4	4.9
3600	0	4.8
3600	0	4.7
3600	0	4.7
3600	0.2	4.7
3600	0.4	4.7
3700	-1	5.1
3700	-1	5
3700	-1	5
3700	-0.8	5
3700	-0.8	4.9
3700	-0.6	4.9
3700	-0.6	4.9
3700	-0.4	4.9
3700	-0.4	4.8
3700	-0.2	4.8
3700	-0.2	4.7
3700	0	4.7
3700	0.2	4.7
3700	0.4	4.7
3700	0.4	4.7
3700	0.4	4.6

T_{eff} (K)	$\log g$ (dex)	[M/H] (dex)
3800	-1	5
3800	-1	4.9
3800	-0.8	4.9
3800	-0.6	4.9
3800	-0.6	4.8
3800	-0.4	4.8
3800	0	4.7
3800	0.2	4.7
3800	0.2	4.6
3900	-1	4.9
3900	-0.8	4.9
3900	-0.8	4.8
3900	-0.4	4.8
3900	-0.4	4.7
3900	-0.2	4.7
3900	0	4.7
3900	0.4	4.7
3900	0.4	4.6
4000	-0.8	4.8
4000	-0.6	4.8
4000	-0.4	4.7
4000	0	4.7
4000	0.2	4.7
4000	0.2	4.6
4000	0.4	4.7

Table A.1. Parameter combination list used for the template normalization. Values taken from PARSEC isochrones (Bressan et al. 2012) for stars with ages between 10^9 and 10^{10} years, and rounded to the nearest multiple of 100 K (for T_{eff}) or 0.1 dex (for $\log g$ and metallicity).

Appendix B: More example synthetic and observed spectra comparisons

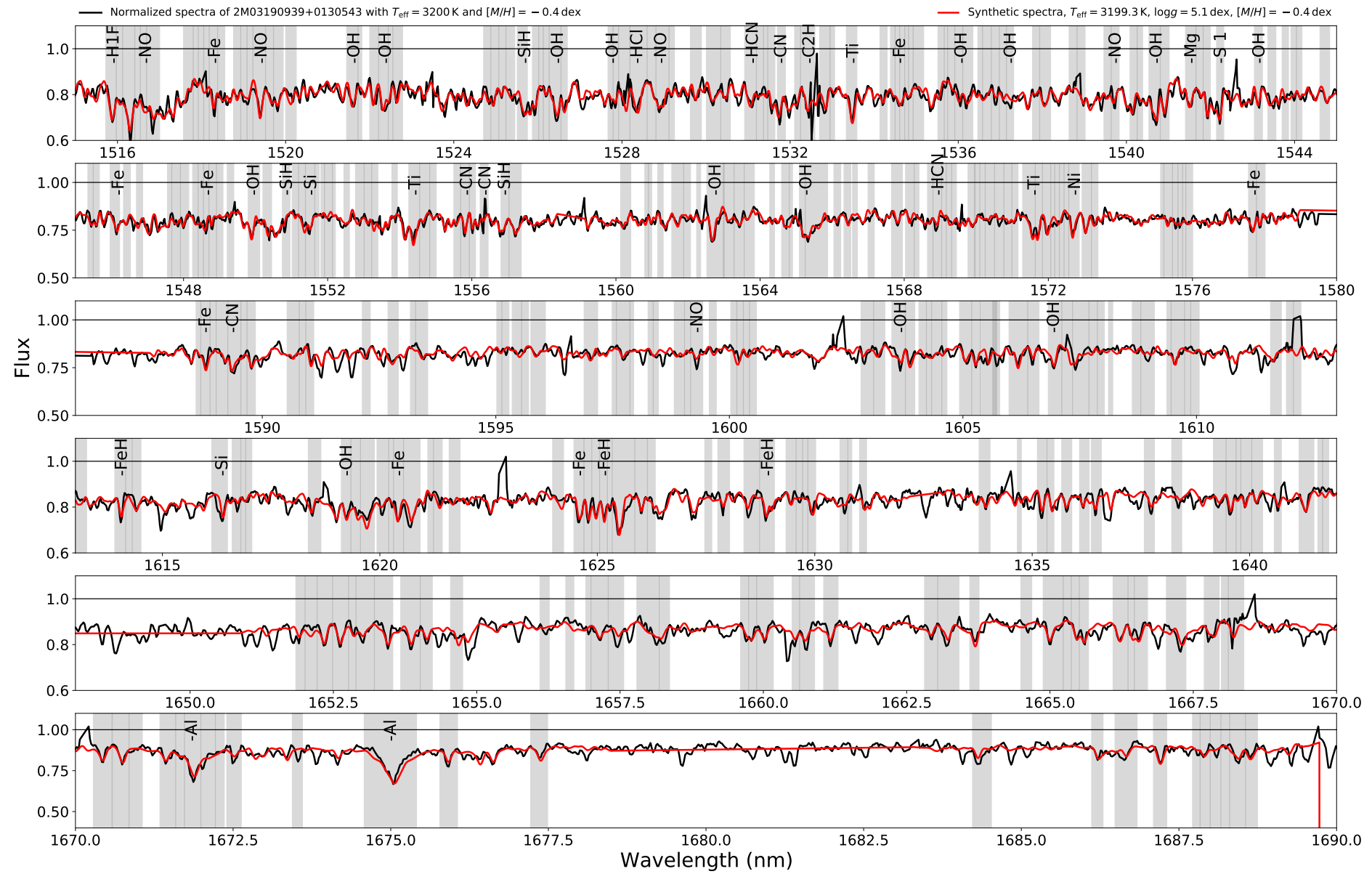


Fig. B.1. Comparison between APOGEE spectra of the star 2M03190939+0130543 (black, normalized using a synthetic spectra with $T_{\text{eff}} = 3200$ K, $\log g = 5.1$ dex and $[M/H] = -0.4$ dex) and the best fitting synthetic spectra (red, straight line) for APOGEE wavelength range. In gray highlight are the areas used for χ^2 minimization by our pipeline's algorithm. The best fitting parameters derived were $T_{\text{eff}} = 3199 \pm 100$ K, $\log g = 5.1 \pm 0.2$ dex, $[M/H] = -0.37 \pm 0.1$ dex. The available ASPCAP parameters are $T_{\text{eff}} = 3287 \pm 60$ K, $\log g = 5.17 \pm 0.14$ dex and $[M/H] = -0.57 \pm 0.02$ dex.

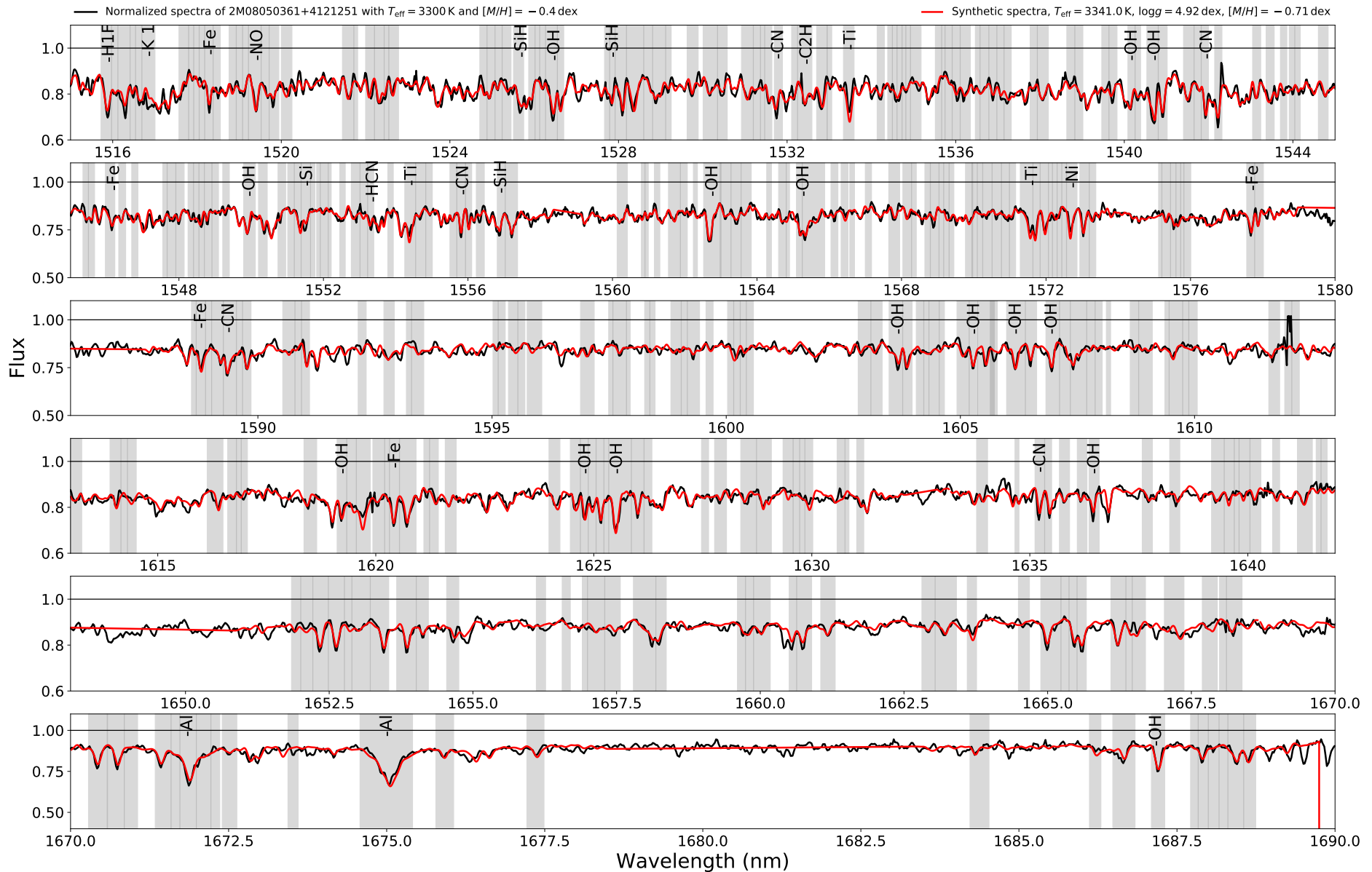


Fig. B.2. Comparison between APOGEE spectra of the star 2M08050361+4121251 (G 111-52, black, normalized using a synthetic spectra with $T_{\text{eff}} = 3400$ K, $\log g = 5.0$ dex and $[M/H] = -0.6$ dex) and the best fitting synthetic spectra (red, straight line) for APOGEE wavelength range. In gray highlight are the areas used for χ^2 minimization by our pipeline's algorithm. The best fitting parameters derived were $T_{\text{eff}} = 3413 \pm 100$ K, $\log g = 4.98 \pm 0.2$ dex, $[M/H] = -0.78 \pm 0.1$ dex.

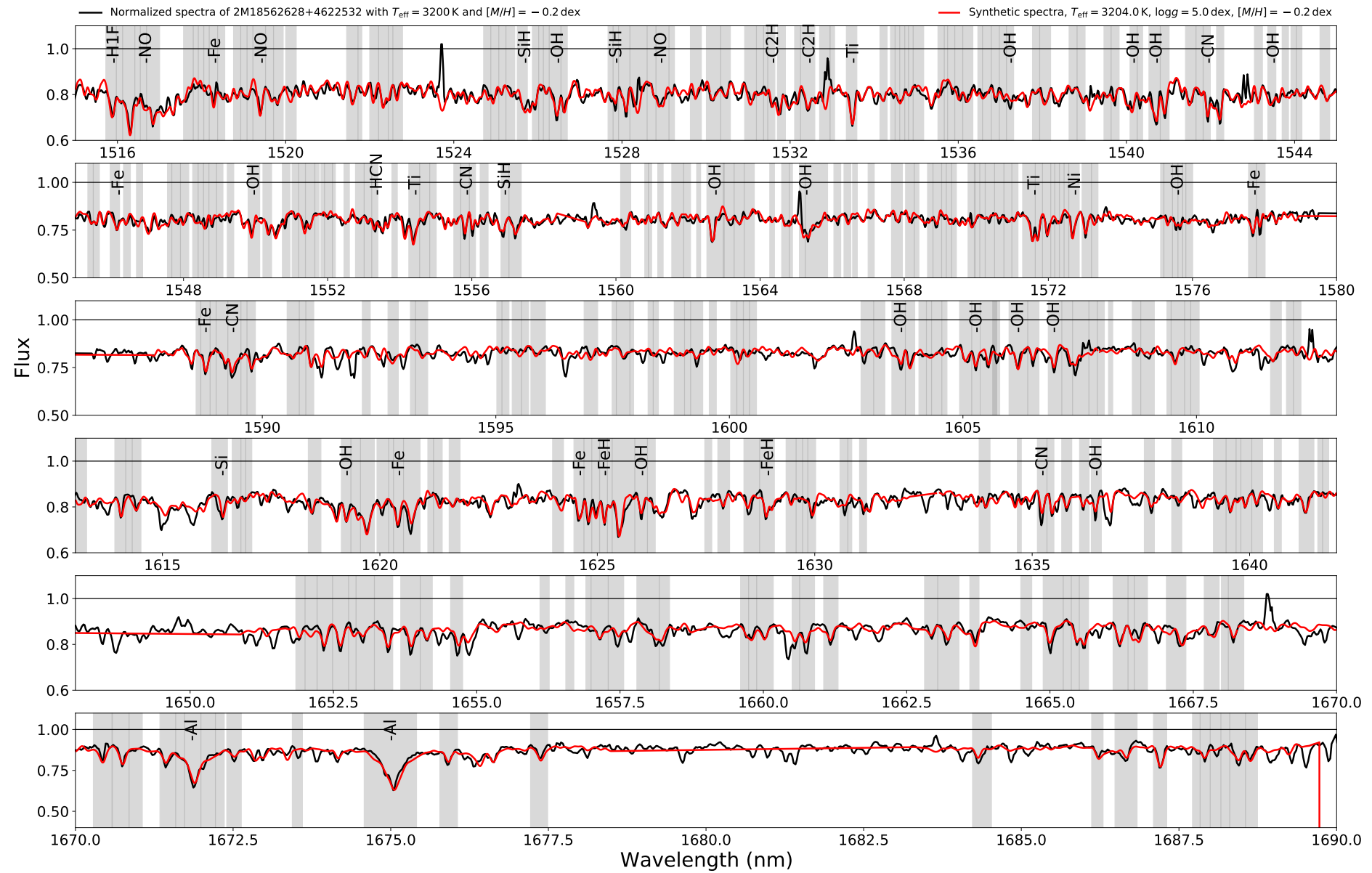


Fig. B.3. Comparison between APOGEE spectra of the star 2M18562628+4622532 (black, normalized using a synthetic spectra with $T_{\text{eff}} = 3200 \text{ K}$, $\log g = 5.0 \text{ dex}$ and $[M/H] = -0.2 \text{ dex}$) and the best fitting synthetic spectra (red, straight line) for APOGEE wavelength range. In gray highlight are the areas used for χ^2 minimization by our pipeline's algorithm. The best fitting parameters derived were $T_{\text{eff}} = 3204 \pm 100 \text{ K}$, $\log g = 4.99 \pm 0.2 \text{ dex}$, $[M/H] = -0.19 \pm 0.1 \text{ dex}$. The available ASPCAP parameters are $T_{\text{eff}} = 3430 \pm 58 \text{ K}$, $\log g = 5.09 \pm 0.13 \text{ dex}$ and $[M/H] = -0.44 \pm 0.02 \text{ dex}$.

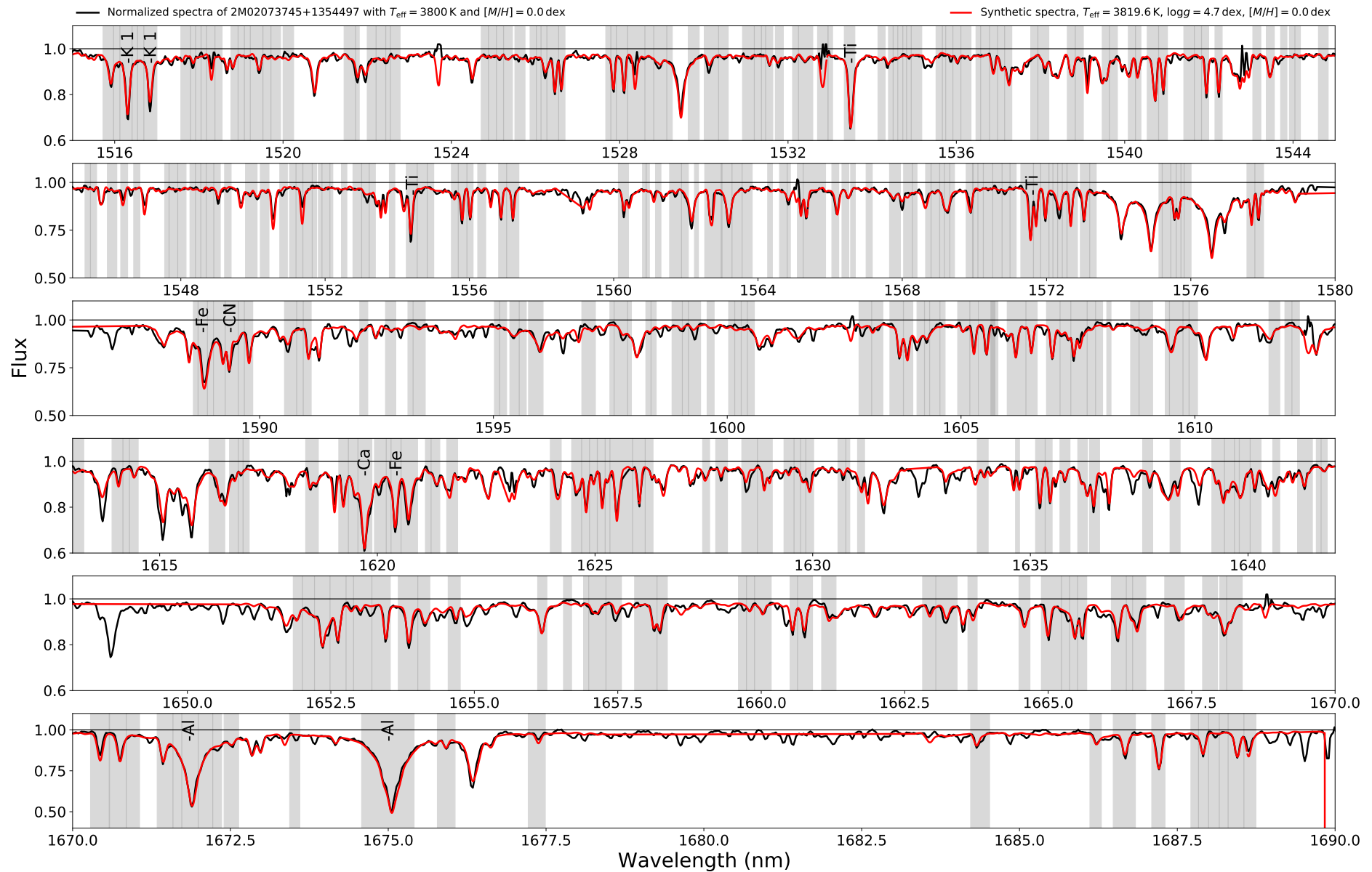


Fig. B.4. Comparison between APOGEE spectra of the star 2M02073745+1354497 (black, normalized using a synthetic spectra with $T_{\text{eff}} = 3800 \text{ K}$, $\log g = 4.7 \text{ dex}$ and $[M/H] = +0.0 \text{ dex}$) and the best fitting synthetic spectra (red, straight line) for APOGEE wavelength range. In gray highlight are the areas used for χ^2 minimization by our pipeline's algorithm. The best fitting parameters derived were $T_{\text{eff}} = 3819 \pm 100 \text{ K}$, $\log g = 4.69 \pm 0.2 \text{ dex}$, $[M/H] = +0.01 \pm 0.1 \text{ dex}$. The available ASPCAP parameters are $T_{\text{eff}} = 3866 \pm 63 \text{ K}$, $\log g = 4.83 \pm 0.11 \text{ dex}$ and $[M/H] = +0.11 \pm 0.01 \text{ dex}$.

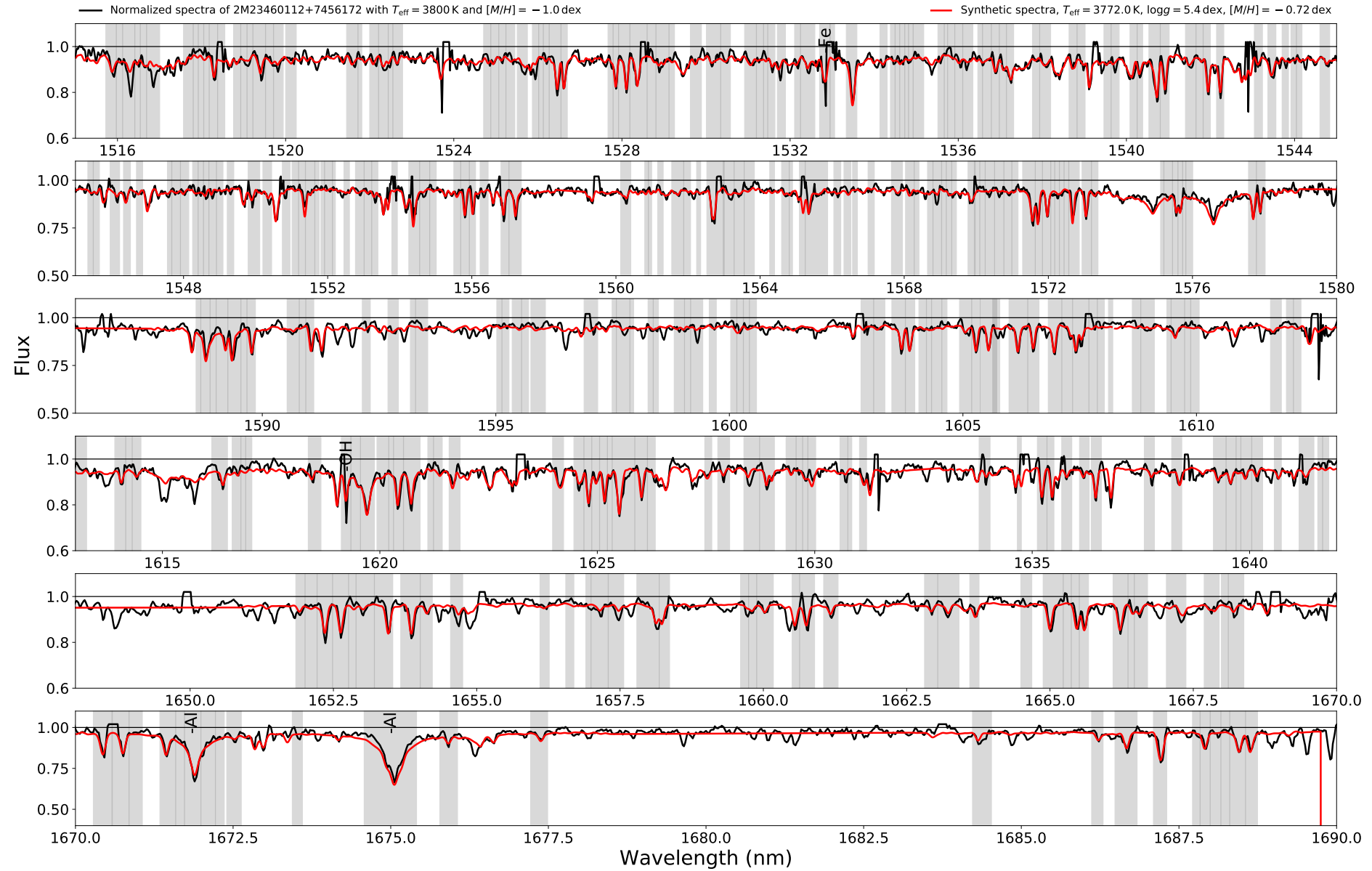


Fig. B.5. Comparison between APOGEE spectra of the star 2M23460112+7456172 (black, normalized using a synthetic spectra with $T_{\text{eff}} = 3600 \text{ K}$, $\log g = 5.0 \text{ dex}$ and $[M/H] = -0.6 \text{ dex}$) and the best fitting synthetic spectra (red, straight line) for APOGEE wavelength range. In gray highlight are the areas used for χ^2 minimization by our pipeline's algorithm. The best fitting parameters derived were $T_{\text{eff}} = 3588 \pm 100 \text{ K}$, $\log g = 5.13 \pm 0.2 \text{ dex}$, $[M/H] = -0.49 \pm 0.1 \text{ dex}$. The available ASPCAP parameters are $T_{\text{eff}} = 3560 \pm 62 \text{ K}$, $\log g = 4.86 \pm 0.13 \text{ dex}$ and $[M/H] = -0.44 \pm 0.02 \text{ dex}$.

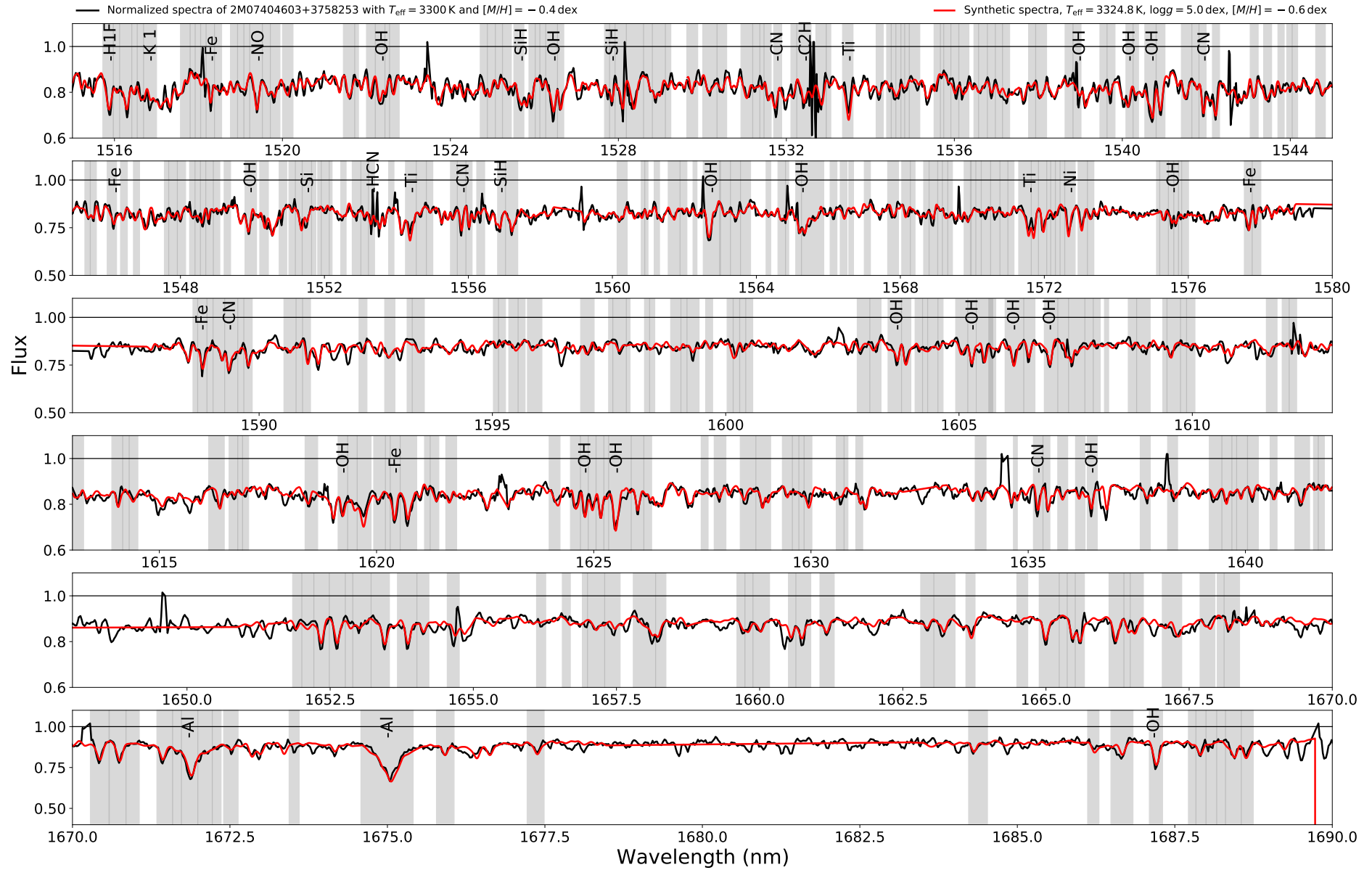


Fig. B.6. Comparison between APOGEE spectra of the star 2M07404603+3758253 (black, normalized using a synthetic spectra with $T_{\text{eff}} = 3300 \text{ K}$, $\log g = 5.0 \text{ dex}$ and $[M/H] = -0.4 \text{ dex}$) and the best fitting synthetic spectra (red, straight line) for APOGEE wavelength range. In gray highlight are the areas used for χ^2 minimization by our pipeline's algorithm. The best fitting parameters derived were $T_{\text{eff}} = 3325 \pm 100 \text{ K}$, $\log g = 4.97 \pm 0.2 \text{ dex}$, $[M/H] = -0.60 \pm 0.1 \text{ dex}$.

Appendix C: Full results for stellar sample, DR16

Table C.1. All derived parameters for stellar sample from APOGEE DR16. Uncertainties in derived parameters are 100 K for T_{eff} , 0.2 dex for $\log g$, and 0.1 dex for $[M/H]$. iSpec output parameters indicated by letter O. Best fitting normalization parameters indicated by letter N.

APOGEE_ID	iSpec Output							Normalization		
	T_{eff}	$\log g$	[M/H]	v_{mic}	v_{mac}	$v \sin i$	χ^2	T_{eff}	$\log g$	[M/H]
2M00004701+1624101	3787	4.77	0.02	0.00	5.83	5.95	0.04	3800	4.7	0
2M00182256+4401222	3695	4.96	-0.54	0.73	6.21	4.31	0.03	3700	4.9	-0.6
2M00204772+5936173	3604	4.79	-0.01	0.76	6.51	1.63	0.04	3600	4.8	0
2M00243855+5119224	3506	4.83	-0.33	0.69	6.91	4.30	0.03	3500	5	-0.4
2M00244054+5511590	3800	4.80	-0.40	0.83	5.79	0.00	0.03	3800	4.8	-0.4
2M00251060+6724193	3715	4.78	-0.29	0.88	6.09	0.00	0.03	3700	4.8	-0.2
2M00262872+6747026	3786	4.66	-0.06	0.05	5.81	4.38	0.03	3800	4.7	0
2M00274401+5330504	3407	4.94	0.06	0.87	7.37	0.28	0.05	3400	4.8	0
2M00313293+6152504	3642	4.77	-0.75	1.71	6.36	0.18	0.04	3600	4.8	-0.4
2M00334916+6712243	3715	4.58	-0.09	0.22	6.06	0.71	0.03	3700	4.7	0
2M00350487+5953079	3209	4.82	-0.02	1.27	8.24	4.88	0.06	3200	4.9	0
2M00363436+5537360	3977	4.73	-0.01	0.00	5.21	6.76	0.04	4000	4.7	0
2M00372598+5133072	3891	4.65	-0.06	0.00	5.46	4.02	0.03	3900	4.7	0
2M00391896+5508132	3410	5.04	-0.85	1.35	7.39	5.49	0.05	3400	5.1	-0.8
2M00444820+1830403	3798	4.92	-0.59	0.92	5.83	2.28	0.02	3800	4.9	-0.6
2M01195227+8409327	3100	5.00	-0.20	0.81	8.84	0.00	0.08	3100	5	-0.2
2M01285381+1803284	3722	4.67	-0.61	1.49	6.04	2.45	0.03	3700	4.8	-0.4
2M02073745+1354497	3820	4.69	0.01	0.00	5.71	2.58	0.04	3800	4.7	0
2M02081366+4949023	2886	4.80	0.25	1.53	9.92	6.18	0.07	2900	5	0.4
2M02090912+1435362	3706	4.92	-0.20	0.49	6.16	2.09	0.03	3700	4.8	-0.2
2M02122001+1249287	3610	5.02	0.19	0.37	6.56	0.00	0.05	3600	4.8	0
2M02361535+0652191	3333	4.71	-0.28	0.77	7.64	3.01	0.06	3300	4.9	-0.2
2M02362715+5528349	3505	5.03	-0.38	1.22	6.98	4.69	0.04	3500	5	-0.4
2M02381299+5542044	4019	4.68	-0.02	0.00	5.08	3.97	0.05	4000	4.7	0
2M02465257+5619505	3534	4.70	-0.32	0.90	6.77	0.25	0.04	3500	4.8	-0.2
2M03044335+6144097	3709	4.91	-0.53	1.78	6.15	0.00	0.05	3700	4.8	-0.4
2M03062774+6254388	3219	5.01	-0.25	1.24	8.25	5.66	0.06	3200	5	-0.2
2M03140624+5728568	3314	4.83	-0.01	0.97	7.75	4.83	0.06	3300	4.9	0
2M03150093+0103083	3804	4.87	-1.05	2.38	5.79	0.00	0.02	3800	4.9	-0.8
2M03152943+5751330	3303	4.91	-0.19	0.85	7.82	2.99	0.06	3300	4.9	-0.2
2M03190939+0130543	3199	5.10	-0.37	1.13	8.39	3.69	0.06	3200	5.1	-0.4
2M03212176+7958022	3600	4.86	-0.35	0.48	6.54	2.92	0.03	3600	4.9	-0.4
2M03215239+6335088	3763	5.04	-0.33	0.87	6.00	0.00	0.03	3800	4.9	-0.6
2M03241544+0928579	3611	4.99	-0.48	1.12	6.54	5.41	0.03	3600	4.9	-0.4
2M03280163+5226180	3894	4.75	-0.19	0.00	5.47	3.24	0.03	3900	4.7	-0.2
2M03355099+7140275	3200	4.93	-0.01	1.16	8.31	3.38	0.08	3200	4.9	0
2M03391302+4635276	3696	4.91	-0.58	1.38	6.19	0.04	0.05	3700	4.9	-0.6
2M03391968+3251001	3416	4.83	0.09	0.64	7.29	5.33	0.05	3400	4.8	0
2M03400164+4638456	3805	4.97	-0.66	1.32	5.83	0.08	0.02	3800	4.9	-0.6
2M03405472+5013200	4034	4.57	-0.10	0.00	5.02	4.25	0.04	4000	4.7	0
2M03431519+5006558	3309	4.88	0.01	0.68	7.78	4.00	0.05	3300	4.9	0
2M03441913+7126195	3604	4.78	0.03	0.00	6.51	2.21	0.04	3600	4.8	0
2M03443389+7125059	3585	5.00	0.04	0.67	6.65	0.00	0.05	3600	4.8	0
2M03481149+3054134	3400	5.00	-0.39	0.85	7.42	0.46	0.06	3400	5	-0.4
2M03553688+5214291	3599	5.08	-0.60	0.97	6.62	0.00	0.04	3600	5	-0.6
2M04125880+5236421	3301	5.00	-0.19	0.85	7.86	3.09	0.06	3300	5	-0.2
2M04244284+4537062	3883	4.70	-0.42	1.33	5.50	0.13	0.03	3900	4.7	-0.4
2M04310001+3647548	3500	4.84	-0.14	1.22	6.94	4.84	0.04	3500	4.9	-0.2
2M04311499+4217111	3602	4.75	-0.01	0.95	6.51	5.04	0.04	3600	4.8	0
2M04311837+3655082	3713	4.68	-0.19	0.22	6.08	2.75	0.03	3700	4.7	-0.2
2M04334819+4227070	3202	4.89	0.00	0.84	8.29	2.46	0.06	3200	4.9	0
2M04340972+4722095	4042	4.70	0.20	0.00	5.01	3.20	0.06	4000	4.7	0.2
2M04342248+4302148	3600	4.71	-0.01	0.79	6.51	0.78	0.03	3600	4.7	0
2M04351236+5821100	3510	4.96	-0.45	1.13	6.93	2.01	0.04	3500	4.9	-0.4
2M04371030+4703549	3714	4.85	-0.65	1.51	6.11	0.12	0.03	3700	4.9	-0.6

Table C.1. continued.

APOGEE_ID	T_{eff}	$\log g$	[M/H]	iSpec Output				Normalization		
				v_{mic}	v_{mac}	$v \sin i$	χ^2	T_{eff}	$\log g$	[M/H]
2M04400301+4620167	3412	4.80	0.06	0.51	7.30	1.82	0.05	3400	4.8	0
2M04422854+5818015	3325	5.00	-0.28	1.29	7.75	5.02	0.05	3300	5	-0.2
2M04443813+3857031	3601	4.84	-0.19	0.75	6.53	1.01	0.03	3600	4.8	-0.2
2M04463593+5900524	3700	4.54	-0.21	0.35	6.11	5.15	0.03	3700	4.7	-0.2
2M04483289+5003109	3501	4.91	-0.19	0.82	6.95	0.87	0.05	3500	4.9	-0.2
2M04552111+5017249	3904	4.71	-0.83	1.71	5.43	2.80	0.02	3900	4.8	-0.8
2M04581599+5017278	3977	4.78	-0.35	0.06	5.22	5.09	0.03	4000	4.7	-0.4
2M04584599+5056378	3892	4.79	-0.17	0.14	5.49	5.90	0.03	3900	4.7	-0.2
2M05011792+4204125	3707	4.70	0.04	0.13	6.10	0.50	0.03	3700	4.7	0
2M05014512+5039319	3695	4.83	-0.33	0.61	6.17	4.79	0.03	3700	4.8	-0.4
2M05145032+4639432	3986	4.71	-0.41	0.00	5.18	5.21	0.03	4000	4.7	-0.4
2M05172841+2531214	3308	4.87	-0.01	0.93	7.78	4.05	0.05	3300	4.9	0
2M05201152+2457212	3690	4.65	-0.02	0.89	6.16	0.00	0.04	3700	4.7	0
2M05222053+3031097	3596	4.93	-0.14	0.58	6.58	0.03	0.04	3600	4.8	-0.2
2M05292729+2724457	3972	4.69	-0.01	0.00	5.22	3.86	0.03	4000	4.7	0
2M05312734-0340356	4005	4.69	0.03	0.00	5.12	2.97	0.05	4000	4.7	0
2M05313731+4128000	3715	4.67	-0.50	1.26	6.07	0.29	0.03	3700	4.8	-0.4
2M05354753+2717497	3710	4.86	-0.24	0.83	6.13	2.59	0.03	3700	4.8	-0.2
2M05370749+4111165	3500	5.02	-0.39	0.87	7.00	2.45	0.04	3500	5	-0.4
2M05392474+4038437	2619	4.93	0.28	2.55	11.53	6.44	0.19	2600	5.1	0.4
2M05394770+2917450	3705	4.69	-0.02	0.00	6.11	2.02	0.03	3700	4.7	0
2M05413073+5329239	3879	4.69	-0.03	0.00	5.51	3.64	0.03	3900	4.7	0
2M05483220+2119180	3417	5.02	-0.28	1.25	7.35	4.98	0.05	3400	4.9	-0.2
2M05483253+2117577	3824	4.62	-0.72	1.08	5.68	0.41	0.03	3800	4.8	-0.6
2M05571864+1708299	3417	4.92	-0.75	1.26	7.31	1.86	0.06	3400	5	-0.6
2M05580690+1557564	3619	4.60	-0.60	1.27	6.42	0.00	0.04	3600	4.8	-0.4
2M06010814+1704162	4063	4.72	-0.37	0.00	4.96	5.08	0.03	4000	4.7	-0.4
2M06025298+3129415	3425	4.87	-0.86	1.62	7.26	3.66	0.05	3400	5	-0.6
2M06043950+2753529	3600	4.80	0.00	0.85	6.53	0.00	0.04	3600	4.8	0
2M06070493+1403109	3301	5.01	-0.20	0.89	7.86	3.44	0.05	3300	5	-0.2
2M06075349+2746207	3886	4.85	-0.17	0.01	5.52	4.95	0.03	3900	4.7	-0.2
2M06102756+2759447	3782	4.69	-0.04	0.00	5.83	4.30	0.03	3800	4.7	0
2M06135175+0631517	3882	4.87	-0.28	0.54	5.54	0.00	0.03	3900	4.8	-0.4
2M06161499+2754094	3696	4.98	-0.24	0.89	6.22	0.00	0.04	3700	4.8	-0.2
2M06183480+2503064	3417	4.85	0.10	0.73	7.29	5.46	0.05	3400	4.8	0
2M06183640+0806535	3891	4.59	-0.43	0.80	5.46	5.20	0.03	3900	4.7	-0.4
2M06234645+0502411	3910	4.68	0.02	0.00	5.41	3.13	0.04	3900	4.7	0
2M06270211+0309473	3797	5.01	-0.59	0.91	5.87	0.01	0.02	3800	4.9	-0.6
2M06274397+0923541	3688	4.89	-0.33	0.72	6.22	0.00	0.03	3700	4.8	-0.4
2M06295663+0934185	3407	4.92	-0.21	1.05	7.36	1.94	0.05	3400	4.9	-0.2
2M06312373+0036445	3792	4.87	-0.54	1.39	5.84	0.00	0.03	3800	4.8	-0.6
2M06320207+3431132	3300	4.90	-0.20	0.82	7.83	0.00	0.06	3300	4.9	-0.2
2M06362535+1830520	3401	5.01	-0.39	0.84	7.41	3.41	0.04	3400	5	-0.4
2M06370004+1515162	3700	4.83	-0.33	0.37	6.16	4.81	0.03	3700	4.8	-0.4
2M06375540+0858594	3204	4.91	-0.01	1.09	8.29	4.69	0.06	3200	4.9	0
2M06385094+1440413	4088	4.67	-0.11	0.00	4.88	7.11	0.05	4000	4.7	0
2M06412818+1545482	3418	4.79	0.08	0.71	7.27	4.71	0.05	3400	4.8	0
2M06421118+0334527	3510	4.83	-0.20	0.79	6.89	2.43	0.04	3500	4.8	-0.2
2M06423361+0239388	3691	4.99	-0.67	0.92	6.24	0.00	0.03	3700	5	-0.8
2M06481555+0326243	2831	5.17	-0.32	1.49	10.37	11.04	0.13	2800	5.2	-0.2
2M06484673-0516193	3877	4.79	-0.19	0.16	5.53	0.88	0.03	3900	4.7	-0.2
2M06505947-0910506	3524	4.95	-0.27	1.15	6.87	0.06	0.04	3500	4.9	-0.2
2M06513673+2023264	3510	4.84	-0.21	0.82	6.90	2.14	0.04	3500	4.8	-0.2
2M06543764+1708058	3615	4.62	-0.57	1.31	6.44	0.00	0.04	3600	4.8	-0.4
2M06572462+0651440	3303	4.92	-0.21	0.94	7.82	3.70	0.06	3300	4.9	-0.2
2M07032384+0132202	4038	4.57	-0.34	0.00	5.01	2.44	0.03	4000	4.7	-0.4
2M07053085+0443219	3910	4.92	-0.86	1.67	5.46	6.34	0.02	3900	4.9	-0.8
2M07062584+0148472	3595	4.77	-0.36	1.05	6.54	0.00	0.04	3600	4.8	-0.4
2M07155314-0101135	3993	4.82	-0.33	0.00	5.18	4.49	0.02	4000	4.7	-0.4
2M07235757-0833017	3500	4.94	-0.19	0.81	6.97	1.92	0.05	3500	4.9	-0.2

Table C.1. continued.

APOGEE_ID	iSpec Output							Normalization		
	T_{eff}	$\log g$	[M/H]	v_{mic}	v_{mac}	$v \sin i$	χ^2	T_{eff}	$\log g$	[M/H]
2M07272450+0513329	3427	4.97	-0.30	1.32	7.29	4.51	0.05	3400	4.9	-0.2
2M07315261-0748360	3904	4.74	-0.33	0.03	5.44	2.16	0.03	3900	4.7	-0.4
2M07320352-0752173	3880	4.88	-0.30	0.49	5.55	0.73	0.03	3900	4.8	-0.4
2M07323759-0813177	3706	4.90	-0.20	0.61	6.15	0.00	0.03	3700	4.8	-0.2
2M07404603+3758253	3325	4.97	-0.61	1.33	7.74	3.15	0.06	3300	5	-0.4
2M07421457+7949418	3204	4.90	0.00	1.00	8.29	5.91	0.06	3200	4.9	0
2M07431638+6642456	3503	4.85	-0.19	0.83	6.93	1.71	0.04	3500	4.9	-0.2
2M07492701+7752423	3302	4.79	-0.01	0.83	7.79	0.00	0.06	3300	4.8	0
2M07551125+4018038	4084	4.62	-0.05	0.00	4.88	8.05	0.04	4000	4.7	0
2M07581269+4118134	3306	4.86	-0.02	0.88	7.79	5.59	0.06	3300	4.9	0
2M08050361+4121251	3413	4.98	-0.78	1.22	7.35	2.46	0.06	3400	5	-0.6
2M08103429-1348514	3612	4.77	-0.19	0.39	6.47	0.00	0.04	3600	4.8	-0.2
2M08595755+0417552	3895	4.81	-0.33	0.57	5.48	0.02	0.03	3900	4.8	-0.4
2M09005033+0514293	3610	4.69	-0.50	1.26	6.46	0.00	0.04	3600	4.8	-0.4
2M09022952+0417072	3520	4.76	-0.28	0.70	6.84	0.08	0.04	3500	4.8	-0.2
2M09142298+5241125	4001	4.71	-0.06	0.00	5.13	4.61	0.04	4000	4.7	0
2M09142485+5241118	4014	4.63	-0.11	0.00	5.08	6.42	0.04	4000	4.7	0
2M09301445+2630250	3401	4.68	0.15	1.16	7.33	1.75	0.06	3400	4.7	0.2
2M10330667+2837490	3309	4.78	-0.01	0.74	7.76	3.65	0.05	3300	4.9	0
2M10371967+3534363	4083	4.75	-0.39	0.00	4.91	4.42	0.03	4000	4.7	-0.4
2M10383323+3529492	3609	4.94	-0.23	0.85	6.53	4.90	0.03	3600	4.8	-0.2
2M10391962+3044566	3601	4.62	-0.19	0.72	6.49	0.00	0.04	3600	4.8	-0.2
2M10401225+3510463	3602	4.93	-0.39	0.86	6.55	0.00	0.03	3600	4.9	-0.4
2M10441137+4500152	3920	4.74	-0.73	1.40	5.39	0.00	0.02	3900	4.8	-0.8
2M10453795+1833111	3863	4.58	-0.07	0.00	5.55	0.91	0.03	3900	4.7	0
2M10463343+1906373	3904	4.71	-0.15	0.00	5.43	4.99	0.03	3900	4.7	-0.2
2M10470720+2004362	3001	5.10	-0.20	0.82	9.39	4.02	0.08	3000	5.1	-0.2
2M10473327+2007406	3508	4.95	-0.21	0.89	6.94	1.58	0.04	3500	4.9	-0.2
2M10475231+2020315	3711	4.60	-0.20	0.16	6.08	0.07	0.03	3700	4.7	-0.2
2M10482152+4451236	3514	5.04	-0.56	1.41	6.95	0.00	0.04	3500	5	-0.4
2M10560279+4858238	3933	4.65	-0.07	0.00	5.33	4.39	0.04	3900	4.7	0
2M10562960+4858264	4071	4.76	0.24	0.00	4.94	3.80	0.05	4000	4.7	0.2
2M10572599+4923562	3691	4.91	-0.15	0.50	6.21	0.00	0.04	3700	4.8	-0.2
2M11021557+4941485	3203	4.98	-0.19	0.93	8.32	1.47	0.03	3200	5	-0.2
2M11032023+3558117	3713	4.85	-0.73	1.44	6.11	0.00	0.04	3700	4.9	-0.6
2M11052903+4331357	3700	4.90	-0.74	1.04	6.18	5.87	0.03	3700	4.9	-0.8
2M11091225-0436249	3891	4.77	-0.22	0.00	5.48	5.07	0.03	3900	4.7	-0.2
2M11152550+0003159	3431	4.70	-0.78	1.36	7.20	0.13	0.05	3400	5	-0.6
2M11202022+0034356	3519	4.90	-0.55	1.17	6.87	0.04	0.05	3500	4.9	-0.4
2M11294200+0405175	3123	5.08	-0.42	1.62	8.75	5.87	0.07	3100	5.1	-0.4
2M11323938+0513167	3898	4.72	-0.19	0.77	5.45	0.70	0.03	3900	4.7	-0.2
2M11353571+0414146	3703	5.01	-0.76	1.22	6.20	0.00	0.03	3700	5	-0.8
2M11452712+2558113	3627	4.87	-0.60	1.54	6.44	2.98	0.05	3600	4.8	-0.4
2M11474440+0048164	3220	5.03	-0.26	1.39	8.26	2.71	0.07	3200	5	-0.2
2M11511794+1829229	3496	4.96	-0.39	1.14	6.99	0.00	0.04	3500	4.9	-0.4
2M11580290+2013015	3308	4.83	-0.01	0.81	7.77	3.85	0.05	3300	4.9	0
2M11585844+2005317	4070	4.66	-0.13	0.00	4.93	5.01	0.04	4000	4.7	0
2M12005016+1938424	3605	4.96	-0.24	0.88	6.55	0.00	0.03	3600	4.8	-0.2
2M12045611+1728119	3507	5.31	-0.76	1.66	7.12	7.53	0.03	3500	5.2	-1
2M12081818+4027012	3967	4.87	-0.28	1.44	5.27	0.00	0.03	4000	4.7	-0.4
2M12082601+4022490	3710	4.60	-0.01	0.00	6.08	3.54	0.03	3700	4.7	0
2M12102152+4026185	3808	4.82	-0.70	1.38	5.77	0.19	0.03	3800	4.8	-0.6
2M12105688+4103275	3903	4.54	-0.59	1.25	5.42	2.92	0.02	3900	4.7	-0.4
2M12110303+4043482	3600	5.00	-0.40	1.02	6.59	2.13	0.04	3600	4.9	-0.4
2M12153222+1515555	3302	4.90	-0.01	0.81	7.82	3.23	0.05	3300	4.9	0
2M12205197+4006468	3691	4.93	-0.81	1.67	6.22	0.03	0.04	3700	4.9	-0.8
2M12212146+5745089	3705	4.81	-0.19	0.76	6.13	1.16	0.03	3700	4.8	-0.2
2M12223238+5730387	3504	4.78	-0.17	0.83	6.91	0.00	0.05	3500	4.8	-0.2
2M12271328+5705444	3693	4.98	-0.36	0.90	6.23	4.07	0.03	3700	4.8	-0.4
2M12301148+5555229	3712	4.94	-0.95	1.72	6.14	4.11	0.03	3700	4.9	-0.8

Table C.1. continued.

APOGEE_ID	iSpec Output							Normalization		
	T_{eff}	$\log g$	[M/H]	v_{mic}	v_{mac}	$v \sin i$	χ^2	T_{eff}	$\log g$	[M/H]
2M12330155+5738113	3631	4.67	-0.62	1.53	6.38	0.07	0.03	3600	4.8	-0.4
2M12505082+1301468	3500	5.00	-0.40	0.80	6.99	0.13	0.04	3500	5	-0.4
2M12523581+4320484	4028	4.68	-0.01	0.07	5.05	3.79	0.04	4000	4.7	0
2M12573249+4057012	3701	4.59	0.00	0.00	6.11	4.92	0.03	3700	4.7	0
2M13085124-0131075	3596	4.88	-0.17	0.88	6.56	1.57	0.04	3600	4.8	-0.2
2M13202492-0139266	3800	4.81	-0.38	0.75	5.79	1.33	0.02	3800	4.8	-0.4
2M13315838+5443452	3709	4.73	-0.06	0.34	6.10	1.40	0.03	3700	4.7	0
2M13421941+1847193	3895	4.78	-0.28	0.05	5.47	0.25	0.02	3900	4.7	-0.4
2M13454354+1453317	3713	4.60	-0.50	1.07	6.07	1.79	0.03	3700	4.8	-0.4
2M13462703+1707100	3695	4.50	-0.19	0.19	6.13	0.00	0.03	3700	4.7	-0.2
2M13481341+2336486	3003	5.09	-0.21	0.95	9.38	4.66	0.10	3000	5.1	-0.2
2M13514938+4157445	3612	4.75	0.04	0.22	6.47	0.34	0.04	3600	4.8	0
2M13525797+3331361	3485	4.62	-0.10	0.36	6.96	4.59	0.04	3500	4.8	-0.2
2M13552585+2556161	4015	4.51	-0.47	0.00	5.07	0.77	0.02	4000	4.7	-0.4
2M13570155+2534378	3800	4.80	-0.36	0.38	5.79	3.29	0.02	3800	4.8	-0.4
2M13572571+3400176	3529	4.97	-0.26	1.03	6.86	7.36	0.04	3500	4.9	-0.2
2M13581901+0119475	3698	4.73	-0.02	0.00	6.14	3.29	0.04	3700	4.7	0
2M14010995+2621429	3927	4.69	-0.20	0.00	5.35	3.00	0.03	3900	4.7	-0.2
2M14022155+2517517	3875	4.80	-0.16	0.02	5.54	0.09	0.03	3900	4.7	-0.2
2M14035430+3008026	3400	4.80	-0.02	0.82	7.35	3.65	0.05	3400	4.8	0
2M14044784+5237559	3171	4.70	0.64	1.10	8.40	5.71	0.07	3100	4.9	0.4
2M14045583+0157230	3701	4.68	-0.17	0.00	6.12	0.00	0.03	3700	4.7	-0.2
2M14130286+0506321	3406	4.88	0.03	0.85	7.35	1.55	0.06	3400	4.8	0
2M14173915+0624144	3389	5.03	-0.34	1.34	7.47	4.80	0.05	3400	5	-0.4
2M14180725+0611519	3302	4.90	-0.02	0.98	7.82	1.75	0.06	3300	4.9	0
2M14385800+1327388	3776	4.66	-0.01	0.38	5.85	1.61	0.04	3800	4.7	0
2M14431906+1120548	3506	4.82	-0.19	0.72	6.91	0.00	0.04	3500	4.8	-0.2
2M14535251+1739448	3816	4.64	-0.50	0.91	5.71	0.32	0.02	3800	4.8	-0.4
2M14540912+4135008	3677	4.91	-0.17	1.07	6.26	0.00	0.04	3700	4.8	-0.2
2M14562713+1755001	3117	5.05	-0.28	1.90	8.77	5.47	0.09	3100	5	-0.2
2M14583396+4216146	3403	4.95	-0.57	1.21	7.38	3.61	0.04	3400	5	-0.6
2M15024283+3211141	3620	4.68	-0.52	1.13	6.43	2.73	0.03	3600	4.8	-0.4
2M15090689+3254449	3416	4.84	0.07	0.81	7.29	3.05	0.05	3400	4.8	0
2M15281240+4340086	3400	5.00	-0.37	1.23	7.42	5.90	0.04	3400	5	-0.4
2M16252459+5418148	3604	5.07	-0.57	0.80	6.60	3.69	0.04	3600	5	-0.6
2M16340737+0038043	3499	5.04	-0.37	0.97	7.01	5.88	0.04	3500	5	-0.4
2M16343937+0051089	3301	5.10	-0.60	0.84	7.90	1.21	0.06	3300	5.1	-0.6
2M16383835+3700273	3302	4.97	-0.18	1.07	7.84	5.06	0.05	3300	5	-0.2
2M16385433+3643018	3896	4.76	-0.26	0.00	5.47	4.50	0.03	3900	4.7	-0.2
2M16440030+3721597	3200	5.10	-0.40	0.80	8.38	1.50	0.07	3200	5.1	-0.4
2M16445239+3644423	3602	4.93	-0.61	1.02	6.56	1.90	0.03	3600	4.9	-0.6
2M16470934+3657361	3788	5.04	-0.54	0.93	5.91	0.00	0.03	3800	4.9	-0.6
2M16495034+4745402	3784	4.69	-0.03	0.30	5.83	3.49	0.03	3800	4.7	0
2M16535528+1138453	4087	4.82	0.22	0.00	4.91	4.76	0.06	4000	4.7	0.2
2M16541202+1154529	3909	4.77	-0.67	0.92	5.43	0.06	0.02	3900	4.8	-0.8
2M16565961+1133582	3399	4.99	-0.59	0.97	7.42	1.11	0.06	3400	5	-0.6
2M16593773+1155377	3924	4.51	-0.29	0.53	5.35	0.00	0.03	3900	4.7	-0.2
2M17014341+1119582	3619	4.81	-0.28	0.86	6.45	0.00	0.03	3600	4.8	-0.2
2M17190292+2340254	3891	4.74	-0.19	0.41	5.48	1.10	0.03	3900	4.7	-0.2
2M17331825+3402191	3995	4.79	-0.37	0.00	5.17	4.91	0.03	4000	4.7	-0.4
2M17362594+6820220	3505	4.64	-0.20	0.68	6.88	0.00	0.02	3500	4.8	-0.2
2M17403275+7256146	4000	4.80	-0.28	0.00	5.15	4.24	0.03	4000	4.7	-0.4
2M17480236+7436562	3202	4.88	-0.01	0.84	8.29	4.31	0.06	3200	4.9	0
2M17491402+4823093	3919	4.80	-0.35	0.06	5.40	2.85	0.03	3900	4.8	-0.4
2M17541820+4758412	3737	4.56	-0.45	1.23	5.98	3.78	0.03	3700	4.7	-0.2
2M17592886+0318233	3912	4.72	-0.03	0.00	5.41	3.59	0.04	3900	4.7	0
2M18055545+0316213	3679	4.76	-0.03	0.57	6.22	0.00	0.04	3700	4.7	0
2M18071735+7402564	3960	4.67	-0.07	0.00	5.25	4.49	0.03	3900	4.7	0
2M18161819+0131277	3510	5.01	-0.43	1.11	6.95	5.53	0.04	3500	5	-0.4
2M18244689-0620311	3507	4.80	-0.19	1.21	6.90	7.99	0.04	3500	4.9	-0.2

Table C.1. continued.

APOGEE_ID	iSpec Output							Normalization		
	T_{eff}	$\log g$	[M/H]	v_{mic}	v_{mac}	$v \sin i$	χ^2	T_{eff}	$\log g$	[M/H]
2M18254864-0258170	3861	4.66	-0.01	0.00	5.56	2.82	0.04	3900	4.7	0
2M18415473+0651285	3502	4.90	-0.19	0.82	6.95	0.78	0.05	3500	4.9	-0.2
2M18424666+5937499	3544	4.90	-0.66	1.88	6.77	0.00	0.04	3500	4.9	-0.4
2M18424688+5937374	3545	4.83	-0.60	1.23	6.75	0.00	0.04	3500	4.9	-0.4
2M18451027+0620158	3871	4.81	-0.16	0.35	5.56	1.77	0.03	3900	4.7	-0.2
2M18543080+4823277	3720	4.73	-0.19	0.00	6.06	4.97	0.03	3700	4.8	-0.2
2M18545777+4730586	3876	4.79	-0.11	0.00	5.54	0.00	0.02	3900	4.7	-0.2
2M18561502+0449049	3719	4.73	-0.74	1.50	6.06	0.56	0.03	3700	4.9	-0.6
2M18562628+4622532	3204	4.99	-0.19	1.01	8.31	4.56	0.07	3200	5	-0.2
2M18571939+0523084	3714	4.63	-0.23	0.62	6.07	0.65	0.03	3700	4.7	-0.2
2M19004176+0310312	3424	4.70	-0.64	1.06	7.23	0.00	0.04	3400	5	-0.6
2M19010098+4522386	3401	4.89	0.00	1.07	7.37	1.62	0.05	3400	4.8	0
2M19034293+3831155	3688	4.71	0.00	0.04	6.17	0.14	0.03	3700	4.7	0
2M19121128+4316106	3628	4.76	-0.60	1.51	6.41	0.79	0.04	3600	4.8	-0.4
2M19165526+0510086	3594	4.67	-0.01	0.49	6.53	0.00	0.02	3600	4.7	0
2M19213157+4317347	3905	4.72	-0.24	0.00	5.43	1.79	0.03	3900	4.7	-0.2
2M19244433+2621167	4167	4.52	-0.04	0.00	4.66	5.98	0.04	4000	4.7	0
2M19250941+1829397	4090	4.69	-0.35	0.00	4.88	7.00	0.03	4000	4.7	-0.4
2M19263973+1736418	3497	5.04	-0.35	1.15	7.02	5.20	0.04	3500	5	-0.4
2M19272432+2619292	3600	5.00	-0.38	0.77	6.59	1.21	0.04	3600	4.9	-0.4
2M19301917+3722350	3876	4.74	0.05	0.00	5.52	0.00	0.04	3900	4.7	0
2M19302719+1723396	3705	4.72	-0.06	0.40	6.11	8.70	0.03	3700	4.7	0
2M19312949+4103513	4107	4.67	0.04	0.00	4.83	0.92	0.03	4000	4.7	0
2M19313868-0658253	3593	4.91	-0.14	0.60	6.58	1.53	0.04	3600	4.8	-0.2
2M19324633-0652178	3511	4.66	-0.24	0.80	6.86	0.16	0.05	3500	4.8	-0.2
2M19325604+1723567	3639	4.77	-0.66	1.53	6.37	0.00	0.04	3600	4.8	-0.4
2M19341617+2553535	3545	4.69	-0.68	1.05	6.72	0.03	0.05	3500	4.9	-0.4
2M19383321+3230175	3481	4.77	-0.07	0.47	7.00	3.39	0.04	3500	4.9	-0.2
2M19390444+2424089	3505	4.91	-0.19	0.80	6.94	0.40	0.04	3500	4.9	-0.2
2M19395886+3950530	3787	4.94	-0.34	1.00	5.88	5.82	0.03	3800	4.8	-0.4
2M19412775+3239512	3634	4.73	-0.70	1.51	6.38	0.07	0.05	3600	4.8	-0.4
2M19420033+4038302	3873	4.66	-0.03	0.10	5.52	5.40	0.03	3900	4.7	0
2M19454969+3223132	3788	4.97	-0.54	0.81	5.89	0.26	0.03	3800	4.9	-0.6
2M19482428+3250327	3615	4.78	-0.75	1.51	6.47	0.00	0.05	3600	4.9	-0.6
2M19485718+5015245	3305	4.84	-0.01	0.94	7.79	3.25	0.06	3300	4.9	0
2M19533423+0503410	3701	4.97	-0.71	1.13	6.19	0.00	0.03	3700	4.9	-0.8
2M19541829+1738289	3301	5.01	-0.39	0.94	7.86	2.80	0.06	3300	5	-0.4
2M19543665+4357180	3919	4.71	-0.32	0.00	5.38	0.18	0.02	3900	4.7	-0.2
2M19585332+0522081	3975	4.94	-0.48	0.04	5.27	1.77	0.02	4000	4.8	-0.6
2M20015056+4500500	3483	4.80	-0.10	0.66	7.00	5.51	0.05	3500	4.9	-0.2
2M20024041+3109447	3614	4.91	-0.26	0.94	6.50	4.69	0.04	3600	4.8	-0.2
2M20032651+2952000	3027	4.76	0.40	0.94	9.14	5.27	0.04	3000	4.9	0.4
2M20053276+3039324	3894	4.60	-0.43	1.20	5.45	0.09	0.03	3900	4.7	-0.4
2M20122244+2043113	3613	4.93	-0.67	1.44	6.51	1.55	0.03	3600	4.9	-0.6
2M20162519+5621561	3688	4.69	0.01	0.13	6.17	2.30	0.04	3700	4.7	0
2M20185746+2704165	3771	5.01	-0.49	0.71	5.96	0.00	0.04	3800	4.9	-0.6
2M20202082+2837583	3789	4.77	0.00	0.00	5.82	3.29	0.04	3800	4.7	0
2M20291663+4507525	3708	4.78	-0.18	0.00	6.11	3.16	0.03	3700	4.8	-0.2
2M20331096+4553299	3603	4.92	-0.38	0.80	6.55	1.63	0.03	3600	4.9	-0.4
2M20584898+5115421	3607	4.92	-0.21	0.67	6.53	0.00	0.04	3600	4.8	-0.2
2M21003448+5156016	3513	4.88	-0.26	1.05	6.90	0.01	0.05	3500	4.8	-0.2
2M21013304+4046208	3432	4.81	-0.35	1.04	7.22	0.00	0.05	3400	4.9	-0.2
2M21074857+2945266	3599	4.92	-0.38	0.86	6.56	0.37	0.03	3600	4.9	-0.4
2M21140743+4924350	3512	5.00	-0.45	1.09	6.94	2.91	0.04	3500	5	-0.4
2M21232573+6734153	3208	4.96	-0.19	0.95	8.29	4.39	0.06	3200	5	-0.2
2M21281491+4654126	3900	4.70	0.00	0.00	5.44	3.21	0.03	3900	4.7	0
2M21400112+5408179	3507	4.84	-0.39	0.93	6.91	3.17	0.04	3500	4.9	-0.4
2M21402935+5400301	3514	4.90	-0.45	1.22	6.90	0.08	0.05	3500	4.9	-0.4
2M21474194+5341222	3711	4.69	-0.15	0.00	6.08	2.48	0.03	3700	4.7	-0.2
2M21561443+3943468	3400	5.00	-0.39	0.82	7.41	0.04	0.05	3400	5	-0.4

Table C.1. continued.

APOGEE_ID	iSpec Output							Normalization		
	T_{eff}	$\log g$	[M/H]	v_{mic}	v_{mac}	$v \sin i$	χ^2	T_{eff}	$\log g$	[M/H]
2M21573509+5026323	3201	4.92	-0.01	0.99	8.30	3.85	0.07	3200	4.9	0
2M22010861+4901108	3976	4.70	-0.06	0.00	5.20	6.44	0.04	3900	4.7	0
2M22563497+1633130	3830	4.71	0.02	0.00	5.67	5.16	0.04	3800	4.7	0
2M23034347+6524293	3218	4.91	0.17	1.17	8.22	5.48	0.06	3200	4.9	0.2
2M23062184+650326	3428	4.73	-0.77	1.29	7.22	0.00	0.05	3400	5	-0.6
2M23110137+4653414	3402	4.71	-0.01	0.90	7.32	0.04	0.05	3400	4.8	0
2M23134861+1227072	3423	4.93	0.19	0.35	7.29	4.75	0.05	3400	4.8	0
2M23165396+6109419	3791	4.90	-0.40	1.38	5.85	0.02	0.03	3800	4.8	-0.4
2M23171589+6110496	3595	4.88	0.02	0.50	6.57	4.04	0.04	3600	4.8	0
2M23175293+6109518	3602	4.94	-0.21	0.84	6.56	0.00	0.04	3600	4.8	-0.2
2M23200542+6356068	3701	4.66	-0.02	0.33	6.12	0.00	0.03	3700	4.7	0
2M23205304+1205009	3503	4.90	-0.39	0.88	6.94	2.46	0.03	3500	4.9	-0.4
2M23212582+6547582	3606	4.96	-0.43	0.94	6.55	2.63	0.03	3600	4.9	-0.4
2M23230603+6211124	3852	4.94	-0.28	0.89	5.65	0.31	0.03	3900	4.8	-0.4
2M23460112+7456172	3589	5.13	-0.49	1.08	6.69	0.00	0.04	3600	5	-0.6
2M23592772+1630288	3410	4.96	0.10	0.67	7.36	4.45	0.05	3400	4.8	0
2M23592810+7506017	3918	4.71	-0.02	0.05	5.39	3.39	0.04	3900	4.7	0
2M23595589+1508091	3576	4.84	-0.25	0.06	6.63	2.74	0.04	3600	4.9	-0.4

Appendix D: Full results for stellar sample, DR14**Table D.1.** All derived parameters for stellar sample from APOGEE DR14. Uncertainties in derived parameters are 100 K for T_{eff} , 0.2 dex for $\log g$, and 0.1 dex for [M/H]. iSpec output parameters indicated by letter O. Best fitting normalization parameters indicated by letter N.

APOGEE_ID	iSpec Output							Normalization		
	T_{eff}	$\log g$	[M/H]	v_{mic}	v_{mac}	$v \sin i$	χ^2	T_{eff}	$\log g$	[M/H]
2M00004701+1624101	3790	4.77	0	0	5.82	5.78	0.16	3800	4.7	0
2M00182256+4401222	3692	4.99	-0.59	0.8	6.24	4.04	0.03	3700	4.9	-0.6
2M00182256+4401222	3702	4.98	-0.56	0.8	6.2	2.54	0.03	3700	4.9	-0.6
2M00204772+5936173	3583	4.72	-0.01	0.61	6.58	4.03	0.21	3600	4.8	0
2M00243855+5119224	3671	5.11	-0.54	0.83	6.37	4.4	0.04	3700	5	-0.8
2M00244054+5511590	3793	4.6	-0.5	0.92	5.78	6.09	0.04	3800	4.8	-0.4
2M00251060+6724193	3702	4.81	-0.31	1.09	6.14	6.17	0.06	3700	4.8	-0.2
2M00262872+6747026	3844	4.8	-0.12	0.56	5.64	5.75	0.18	3900	4.7	-0.2
2M00274401+5330504	3390	5	0.07	0.79	7.46	5.4	0.12	3400	4.8	0
2M00313293+6152504	3630	4.74	-0.8	1.65	6.4	5.07	0.09	3600	4.8	-0.4
2M00334916+6712243	3671	4.54	-0.04	0.31	6.22	3.6	0.19	3700	4.7	0
2M00350487+5953079	3208	4.86	-0.01	1.36	8.25	11.48	0.29	3200	4.9	0
2M00363436+5537360	3967	4.74	0	0	5.24	5	0.26	4000	4.7	0
2M00372598+5133072	3859	4.6	-0.07	0	5.56	5.12	0.11	3900	4.7	0
2M00391896+5508132	3329	5.06	-0.75	1.3	7.75	5.13	0.23	3300	5.1	-0.6
2M00444820+1830403	3784	4.93	-0.61	1.01	5.88	5.04	0.04	3800	4.9	-0.6
2M01195227+8409327	3125	5.01	-0.23	1.03	8.71	5.09	0.19	3100	5	-0.2
2M01285381+1803284	3787	4.9	-0.71	1.93	5.86	4.66	0.03	3800	4.8	-0.6
2M02073745+1354497	3800	4.71	0.02	0	5.77	5.02	0.15	3800	4.7	0
2M02081366+4949023	3007	5.11	-0.4	1.66	9.37	6.46	0.09	3000	5.1	-0.4
2M02090912+1435362	3676	4.9	-0.18	0.39	6.26	4.7	0.09	3700	4.8	-0.2
2M02122001+1249287	3590	5	0.17	0.04	6.63	4.99	0.09	3600	4.8	0
2M02361535+0652191	3310	4.79	-0.22	0.69	7.76	3.93	0.07	3300	4.9	-0.2
2M02362715+5528349	3499	5.06	-0.42	1.27	7.02	5.78	0.08	3500	5	-0.4
2M02381299+5542044	4055	4.69	-0.03	0	4.97	5.19	0.17	4000	4.7	0
2M02465257+5619505	3504	4.66	-0.28	0.96	6.89	4.7	0.12	3500	4.8	-0.2
2M03044335+6144097	3602	4.81	-0.49	1.49	6.52	3.3	0.11	3600	4.8	-0.4
2M03062774+6254388	3298	5.19	-0.26	1.21	7.96	5.29	0.09	3300	5	-0.2
2M03140624+5728568	3302	4.85	-0.02	1.02	7.81	6.85	0.08	3300	4.9	0
2M03150093+0103083	3700	4.7	-1.08	1.94	6.13	5.72	0.04	3700	4.9	-0.8
2M03152943+5751330	3384	5.11	-0.32	1.34	7.53	5.32	0.08	3400	5	-0.4
2M03190939+0130543	2973	4.7	0.23	1.12	9.42	11.54	0.08	3000	4.9	0.4

Table D.1. continued.

APOGEE_ID	T_{eff}	$\log g$	[M/H]	iSpec Output				Normalization		
				v_{mic}	v_{mac}	$v \sin i$	χ^2	T_{eff}	$\log g$	[M/H]
2M03212176+7958022	3585	4.87	-0.36	0.62	6.6	4.65	0.3	3600	4.9	-0.4
2M03215239+6335088	3751	5.05	-0.35	0.79	6.04	4.81	0.04	3800	4.9	-0.6
2M03241544+0928579	3592	4.98	-0.55	1.09	6.61	5.63	0.11	3600	5	-0.6
2M03280163+5226180	3850	4.67	-0.19	0	5.6	3.42	0.05	3900	4.7	-0.2
2M03355099+7140275	3196	4.95	-0.01	1.19	8.34	4.7	0.22	3200	4.9	0
2M03391302+4635276	3774	5.05	-0.71	1.63	5.97	0.67	0.07	3800	4.9	-0.6
2M03391968+3251001	3401	4.88	0.08	0.66	7.37	5.02	0.07	3400	4.8	0
2M03400164+4638456	3697	4.79	-0.68	0.98	6.16	5.33	0.1	3700	4.9	-0.6
2M03405472+5013200	4017	4.57	-0.11	0	5.07	4.95	0.19	4000	4.7	0
2M03431519+5006558	3299	4.93	0	0.91	7.84	7.94	0.18	3300	4.9	0
2M03441913+7126195	3657	4.86	0.02	0.17	6.32	5.05	0.06	3700	4.7	0
2M03443389+7125059	3567	5	0	0.71	6.72	5.91	0.07	3600	4.8	0
2M03481149+3054134	3397	5.07	-0.39	1.06	7.46	3.79	0.08	3400	5	-0.4
2M03553688+5214291	3502	5.02	-0.58	1.26	6.99	5.24	0.13	3500	5	-0.6
2M04125880+5236421	3302	5.01	-0.19	0.93	7.86	3.67	0.54	3300	5	-0.2
2M04244284+4537062	3865	4.69	-0.44	1.29	5.55	5.77	0.05	3900	4.7	-0.4
2M04310001+3647548	3492	4.91	-0.17	1.28	6.99	6.01	0.24	3500	4.9	-0.2
2M04311499+4217111	3581	4.72	-0.01	1.01	6.59	5.95	0.17	3600	4.8	0
2M04311837+3655082	3678	4.64	-0.16	0	6.2	5.08	0.13	3700	4.7	-0.2
2M04334819+4227070	3130	4.85	0.27	0.96	8.63	5.34	0.09	3100	4.9	0.2
2M04340972+4722095	4080	4.69	0.17	0	4.9	5.03	0.15	4000	4.7	0.2
2M04342248+4302148	3592	4.73	-0.05	0.58	6.54	3.36	0.08	3600	4.8	0
2M04351236+5821100	3503	4.96	-0.49	1.16	6.96	4.33	0.17	3500	4.9	-0.4
2M04371030+4703549	3698	4.87	-0.71	1.57	6.17	4.94	0.04	3700	4.9	-0.6
2M04400301+4620167	3396	4.83	0.05	0.62	7.38	4.76	0.07	3400	4.8	0
2M04422854+5818015	3301	5.01	-0.21	0.95	7.87	5.25	0.19	3300	5	-0.2
2M04443813+3857031	3580	4.9	-0.15	0.86	6.63	5.04	0.11	3600	4.8	-0.2
2M04463593+5900524	3668	4.54	-0.17	0.41	6.23	4.22	0.1	3700	4.7	-0.2
2M04483289+5003109	3482	4.92	-0.15	0.94	7.04	3.89	0.09	3500	4.9	-0.2
2M04552111+5017249	3884	4.69	-0.85	1.64	5.49	4.3	0.04	3900	4.8	-0.8
2M04581599+5017278	3958	4.8	-0.31	0.12	5.28	3.66	0.07	4000	4.7	-0.4
2M04584599+5056378	3860	4.77	-0.17	0	5.59	5.17	0.17	3900	4.7	-0.2
2M05011792+4204125	3680	4.68	0.02	0	6.2	5.13	0.13	3700	4.7	0
2M05014512+5039319	3681	4.8	-0.37	0.68	6.22	3.11	0.07	3700	4.8	-0.4
2M05145032+4639432	3968	4.72	-0.4	0.29	5.23	3.8	0.06	4000	4.7	-0.4
2M05172841+2531214	3298	4.86	-0.01	1.01	7.83	6.16	0.14	3300	4.9	0
2M05201152+2457212	3669	4.57	-0.07	0.84	6.23	5.21	0.17	3700	4.7	0
2M05222053+3031097	3582	5	-0.03	0.77	6.66	6.41	0.15	3600	4.8	0
2M05292729+2724457	3959	4.68	-0.02	0	5.25	4.9	0.12	4000	4.7	0
2M05312734-0340356	3994	4.72	0.04	0	5.15	4.13	0.05	4000	4.7	0
2M05313731+4128000	3702	4.69	-0.5	1.34	6.12	5.47	0.05	3700	4.8	-0.4
2M05354753+2717497	3685	4.84	-0.24	0.88	6.22	5.35	0.08	3700	4.8	-0.2
2M05370749+4111165	3413	4.97	-0.28	1.03	7.35	5.87	0.06	3400	4.9	-0.2
2M05392474+4038437	1950	4.9	0.3	1.94	16.22	6.4	0.22	2300	5.1	0.4
2M05394770+2917450	3668	4.64	-0.02	0	6.24	3.75	0.11	3700	4.7	0
2M05413073+5329239	3872	4.7	-0.03	0	5.53	4.32	0.03	3900	4.7	0
2M05483220+2119180	3399	5.06	-0.22	0.99	7.45	4.55	0.13	3400	4.9	-0.2
2M05483253+2117577	3795	4.62	-0.72	1.1	5.78	5.13	0.03	3800	4.8	-0.6
2M05571864+1708299	3427	4.94	-0.87	1.58	7.28	4.53	0.12	3400	5	-0.6
2M05580690+1557564	3609	4.6	-0.63	1.46	6.46	5.53	0.09	3600	4.8	-0.4
2M06010814+1704162	4033	4.76	-0.33	0	5.05	6.04	0.06	4000	4.7	-0.4
2M06025298+3129415	3435	4.85	-1	1.83	7.21	5.33	0.06	3400	5	-0.6
2M06043950+2753529	3590	4.71	-0.04	0.65	6.55	6.16	0.1	3600	4.7	0
2M06070493+1403109	3295	5.1	-0.23	1.22	7.93	5	0.1	3300	5	-0.2
2M06075349+2746207	3857	4.82	-0.15	0	5.6	5.26	0.12	3900	4.7	-0.2
2M06102756+2759447	3756	4.71	-0.02	0.1	5.93	3.95	0.09	3800	4.7	0
2M06135175+0631517	3855	4.89	-0.26	0.68	5.63	6.23	0.1	3900	4.8	-0.4
2M06161499+2754094	3674	5	-0.23	0.91	6.3	5.57	0.08	3700	4.8	-0.2
2M06183480+2503064	3400	4.87	0.07	0.81	7.37	4.44	0.1	3400	4.8	0
2M06183640+0806535	3865	4.58	-0.42	0.66	5.54	5.14	0.06	3900	4.7	-0.4

Table D.1. continued.

APOGEE_ID	iSpec Output							Normalization		
	T_{eff}	$\log g$	[M/H]	v_{mic}	v_{mac}	$v \sin i$	χ^2	T_{eff}	$\log g$	[M/H]
2M06234645+0502411	3886	4.65	0.01	0	5.48	4.42	0.2	3900	4.7	0
2M06270211+0309473	3693	4.94	-0.57	0.82	6.21	5.18	0.05	3700	4.9	-0.6
2M06274397+0923541	3670	4.91	-0.3	0.68	6.29	3.9	0.12	3700	4.8	-0.4
2M06295663+0934185	3401	4.94	-0.23	1.12	7.39	4.15	0.09	3400	4.9	-0.2
2M06312373+0036445	3703	4.77	-0.49	1.04	6.13	3.16	0.07	3700	4.8	-0.4
2M06320207+3431132	3301	5.01	-0.2	0.94	7.86	4.21	0.08	3300	5	-0.2
2M06362535+1830520	3398	5.07	-0.4	1.04	7.45	5.13	0.12	3400	5	-0.4
2M06370004+1515162	3676	4.82	-0.32	0	6.24	5.09	0.06	3700	4.8	-0.4
2M06375540+0858594	3199	4.9	0	0.98	8.31	5.23	0.07	3200	4.9	0
2M06385094+1440413	4076	4.69	-0.13	0	4.91	10.78	0.11	4000	4.7	0
2M06412818+1545482	3400	4.79	0.06	0.72	7.35	5.31	0.13	3400	4.8	0
2M06421118+0334527	3498	4.85	-0.24	0.92	6.95	6.6	0.35	3500	4.8	-0.2
2M06423361+0239388	3786	5.1	-0.75	1.29	5.95	5.2	0.07	3800	4.9	-0.8
2M06481555+0326243	2792	4.8	0.27	2.64	10.45	7.81	0.3	2800	5	0.4
2M06484673-0516193	3841	4.76	-0.17	0	5.65	4.43	0.09	3900	4.7	-0.2
2M06505947-0910506	3497	4.95	-0.23	0.95	6.98	3.39	0.16	3500	4.9	-0.2
2M06513673+2023264	3584	4.99	-0.39	1.18	6.64	4.06	0.23	3600	4.9	-0.4
2M06543764+1708058	3606	4.65	-0.58	1.37	6.47	3.65	0.07	3600	4.8	-0.4
2M06572462+0651440	3310	5.04	-0.25	1.17	7.83	4.57	0.07	3300	5	-0.2
2M07032384+0132202	4023	4.55	-0.34	0	5.05	4.54	0.03	4000	4.7	-0.4
2M07053085+0443219	3892	5.01	-0.87	1.85	5.55	5.31	0.04	3900	4.9	-0.8
2M07062584+0148472	3579	4.77	-0.35	1.07	6.6	5.91	0.08	3600	4.8	-0.4
2M07155314-0101135	3974	4.77	-0.37	0	5.22	6.16	0.08	4000	4.7	-0.4
2M07235757-0833017	3467	4.95	-0.1	0.77	7.11	6.74	0.17	3500	4.9	-0.2
2M07272450+0513329	3399	4.95	-0.23	1.08	7.4	3.89	0.05	3400	4.9	-0.2
2M07315261-0748360	3869	4.73	-0.29	0	5.55	4.03	0.07	3900	4.7	-0.4
2M07320352-0752173	3848	4.92	-0.26	0.57	5.66	5.19	0.06	3900	4.8	-0.4
2M07323759-0813177	3676	4.85	-0.19	0.7	6.25	3.24	0.11	3700	4.8	-0.2
2M07404603+3758253	3325	5.06	-0.62	1.49	7.77	4.52	0.09	3300	5	-0.4
2M07421457+7949418	3189	5	0	1.1	8.39	3.83	0.07	3200	4.9	0
2M07431638+6642456	3485	4.74	-0.15	0.64	6.98	5.19	0.06	3500	4.9	-0.2
2M07492701+7752423	3292	4.75	-0.01	0.8	7.83	3.42	0.09	3300	4.8	0
2M07551125+4018038	4066	4.64	-0.06	0	4.94	7.42	0.11	4000	4.7	0
2M07581269+4118134	3302	4.92	-0.07	0.88	7.83	6.29	0.34	3300	4.9	0
2M08050361+4121251	3341	4.92	-0.71	1.32	7.65	5.13	0.08	3300	5	-0.4
2M08103429-1348514	3678	4.92	-0.21	0.77	6.26	5.29	0.14	3700	4.8	-0.2
2M08595755+0417552	3848	4.85	-0.24	0.41	5.64	3.16	0.07	3900	4.8	-0.4
2M09005033+0514293	3603	4.72	-0.5	1.3	6.5	6.07	0.14	3600	4.8	-0.4
2M09022952+0417072	3589	4.94	-0.43	1.03	6.61	2.41	0.06	3600	4.9	-0.4
2M09142298+5241125	3993	4.68	-0.08	0	5.15	5.81	0.03	4000	4.7	0
2M09142485+5241118	3996	4.63	-0.11	0	5.14	4.47	0.04	4000	4.7	0
2M09301445+2630250	3385	4.66	0.14	1.13	7.39	5.08	0.25	3400	4.7	0.2
2M10330667+2837490	3298	4.88	0	0.87	7.83	4.05	0.06	3300	4.9	0
2M10371967+3534363	4067	4.82	-0.34	0	4.97	5.35	0.07	4000	4.7	-0.4
2M10383323+3529492	3591	4.96	-0.22	0.77	6.6	4.83	0.14	3600	4.8	-0.2
2M10391962+3044566	3684	4.87	-0.22	1.25	6.23	4.83	0.05	3700	4.8	-0.2
2M10401225+3510463	3682	5.06	-0.54	1.17	6.3	2.69	0.04	3700	4.9	-0.6
2M10441137+4500152	3804	4.66	-0.63	1.1	5.75	3.94	0.02	3800	4.8	-0.6
2M10453795+1833111	3852	4.61	-0.05	0	5.59	4.53	0.1	3900	4.7	0
2M10463343+1906373	3783	4.61	-0.02	0	5.82	4.91	0.07	3800	4.7	0
2M10470720+2004362	2988	4.8	0.01	1.44	9.36	9.36	0.09	3000	5	0.2
2M10473327+2007406	3498	5.03	-0.22	1.01	7.01	3.84	0.16	3500	4.9	-0.2
2M10475231+2020315	3673	4.6	-0.17	0.36	6.22	2.63	0.08	3700	4.7	-0.2
2M10482152+4451236	3416	5	-0.5	1.26	7.35	5.48	0.07	3400	5	-0.4
2M10560279+4858238	3915	4.69	-0.03	0.05	5.39	4.52	0.14	3900	4.7	0
2M10562960+4858264	4045	4.75	0.21	0	5.01	4.78	0.11	4000	4.7	0.2
2M10572599+4923562	3672	4.89	-0.15	0.45	6.27	3.48	0.11	3700	4.8	-0.2
2M11021557+4941485	3292	5.11	-0.19	1.07	7.95	5.5	0.06	3300	5	-0.2
2M11032023+3558117	3702	4.88	-0.76	1.54	6.16	5.13	0.05	3700	4.9	-0.6
2M11052903+4331357	3705	5.03	-0.7	1.27	6.2	5.23	0.03	3700	4.9	-0.6

Table D.1. continued.

APOGEE_ID	T_{eff}	$\log g$	[M/H]	iSpec Output				Normalization		
				v_{mic}	v_{mac}	$v \sin i$	χ^2	T_{eff}	$\log g$	[M/H]
2M11091225-0436249	3882	4.75	-0.21	0.24	5.51	2.74	0.15	3900	4.7	-0.2
2M11152550+0003159	3430	4.87	-0.83	1.88	7.24	6.5	0.1	3400	5	-0.6
2M11202022+0034356	3511	4.9	-0.56	1.15	6.91	6.28	0.09	3500	4.9	-0.4
2M11294200+0405175	3116	5.13	-0.4	1.34	8.81	4.59	0.09	3100	5.1	-0.4
2M11323938+0513167	3871	4.72	-0.17	0.77	5.54	4.1	0.05	3900	4.7	-0.2
2M11353571+0414146	3795	5.1	-0.87	1.43	5.91	6.06	0.05	3800	4.9	-0.8
2M11452712+2558113	3614	4.88	-0.6	1.39	6.49	1.81	0.12	3600	4.8	-0.4
2M11474440+0048164	3203	5.04	-0.2	1.09	8.34	6.76	0.08	3200	5	-0.2
2M11511794+1829229	3493	5	-0.39	1.14	7.02	3.43	0.12	3500	4.9	-0.4
2M11580290+2013015	3306	4.87	-0.18	1.05	7.79	5.53	0.06	3300	5	-0.2
2M11585844+2005317	4052	4.65	-0.15	0	4.98	5.46	0.08	4000	4.7	0
2M12005016+1938424	3491	4.76	-0.2	0.67	6.96	5.59	0.04	3500	4.8	-0.2
2M12045611+1728119	3509	5.4	-0.78	1.88	7.17	17.47	0.07	3500	5.2	-1
2M12081818+4027012	3892	4.69	-0.26	0.96	5.46	3.55	0.04	3900	4.7	-0.2
2M12082601+4022490	3691	4.62	0	0	6.15	5.49	0.1	3700	4.7	0
2M12102152+4026185	3789	4.87	-0.71	1.51	5.85	5.39	0.04	3800	4.8	-0.6
2M12105688+4103275	3876	4.51	-0.59	1.2	5.5	4.96	0.11	3900	4.7	-0.4
2M12110303+4043482	3593	5	-0.42	0.98	6.62	3.54	0.08	3600	4.9	-0.4
2M12153222+1515555	3300	4.9	0	0.83	7.83	4.09	0.08	3300	4.9	0
2M12205197+4006468	3602	4.8	-0.74	1.41	6.52	0	0.08	3600	4.9	-0.6
2M12212146+5745089	3679	4.77	-0.15	0.69	6.22	3.91	0.11	3700	4.8	-0.2
2M12223238+5730387	3483	4.8	-0.19	0.85	7	5.02	0.07	3500	4.8	-0.2
2M12271328+5705444	3680	5	-0.36	0.92	6.28	6.42	0.09	3700	4.8	-0.4
2M12301148+5555229	3691	4.7	-1.13	1.65	6.16	4.52	0.03	3700	4.9	-0.8
2M12330155+5738113	3623	4.69	-0.68	1.56	6.42	5.35	0.04	3600	4.8	-0.4
2M12505082+1301468	3487	5.04	-0.39	1.05	7.06	4.55	0.04	3500	5	-0.4
2M12523581+4320484	4025	4.67	-0.02	0	5.06	5.11	0.07	4000	4.7	0
2M12573249+4057012	3674	4.55	0	0	6.21	4.79	0.05	3700	4.7	0
2M13085124-0131075	3570	4.94	-0.12	0.98	6.68	5.29	0.12	3600	4.8	-0.2
2M13202492-0139266	3772	4.84	-0.35	0.5	5.9	3.75	0.1	3800	4.8	-0.4
2M13315838+5443452	3686	4.73	-0.05	0.3	6.19	2.88	0.1	3700	4.7	0
2M13421941+1847193	3879	4.83	-0.27	0	5.54	5.17	0.03	3900	4.8	-0.4
2M13454354+1453317	3698	4.62	-0.5	1.05	6.12	4.91	0.03	3700	4.8	-0.4
2M13462703+1707100	3666	4.5	-0.17	0.41	6.24	2.16	0.08	3700	4.7	-0.2
2M13481341+2336486	3005	5.09	-0.36	1.28	9.37	7.72	0.13	3000	5.1	-0.4
2M13514938+4157445	3599	4.82	0.06	0	6.54	3.38	0.12	3600	4.8	0
2M13525797+3331361	3668	5	-0.2	0.96	6.33	5.67	0.05	3700	4.8	-0.2
2M13552585+2556161	4007	4.5	-0.48	0	5.1	4.3	0.03	4000	4.7	-0.4
2M13570155+2534378	3776	4.83	-0.36	0.33	5.88	4.24	0.08	3800	4.8	-0.4
2M13572571+3400176	3499	4.97	-0.23	0.89	6.98	5.63	0.07	3500	4.9	-0.2
2M13581901+0119475	3673	4.7	-0.01	0.45	6.23	4.39	0.12	3700	4.7	0
2M14010995+2621429	3893	4.66	-0.19	0	5.46	4.3	0.08	3900	4.7	-0.2
2M14022155+2517517	3862	4.82	-0.13	0	5.59	5.3	0.06	3900	4.7	-0.2
2M14035430+3008026	3388	4.81	-0.01	0.79	7.41	5.3	0.08	3400	4.8	0
2M14044784+5237559	3589	4.81	-0.23	0.98	6.57	1.51	0.06	3600	4.8	-0.2
2M14045583+0157230	3677	4.68	-0.15	0.17	6.21	2.33	0.07	3700	4.7	-0.2
2M14130286+0506321	3390	4.9	0.02	0.91	7.42	3.43	0.15	3400	4.8	0
2M14173915+0624144	3298	4.95	-0.07	0.93	7.86	5.69	0.07	3300	4.9	0
2M14180725+0611519	3295	4.89	-0.01	0.94	7.85	3.78	0.07	3300	4.9	0
2M14385800+1327388	3761	4.66	-0.03	0.42	5.9	3.37	0.06	3800	4.7	0
2M14431906+1120548	3490	4.9	-0.2	0.77	7	3.36	0.06	3500	4.8	-0.2
2M14535251+1739448	3795	4.64	-0.5	0.83	5.78	4.87	0.08	3800	4.8	-0.4
2M14540912+4135008	3669	4.96	-0.16	1.11	6.31	5.09	0.06	3700	4.8	-0.2
2M14562713+1755001	3116	5.06	-0.28	1.91	8.78	6.06	0.15	3100	5	-0.2
2M14583396+4216146	3497	5.16	-0.7	1.5	7.07	4.51	0.06	3500	5.1	-0.8
2M15010818+2250020	1964	4.9	0.24	3.99	16.11	0	0.19	2300	5.1	0.4
2M15024283+3211141	3608	4.71	-0.5	1.08	6.47	3.09	0.05	3600	4.8	-0.4
2M15090689+3254449	3397	4.87	0.06	0.8	7.38	5.47	0.1	3400	4.8	0
2M15281240+4340086	3305	4.9	-0.21	1	7.81	6.6	0.13	3300	4.9	-0.2
2M16252459+5418148	3607	5.12	-0.62	0.97	6.61	4.61	0.05	3600	5	-0.6

Table D.1. continued.

APOGEE_ID	iSpec Output							Normalization		
	T_{eff}	$\log g$	[M/H]	v_{mic}	v_{mac}	$v \sin i$	χ^2	T_{eff}	$\log g$	[M/H]
2M16340737+0038043	3488	5.08	-0.35	1.06	7.08	4.63	0.1	3500	5	-0.4
2M16343937+0051089	3311	5.13	-0.68	1.52	7.87	6.45	0.08	3300	5.1	-0.6
2M16383835+3700273	3317	5.06	-0.1	1.12	7.81	6.33	0.14	3300	4.9	0
2M16385433+3643018	3872	4.76	-0.26	0	5.54	5.8	0.1	3900	4.7	-0.4
2M16440030+3721597	3487	5.4	-0.72	1.06	7.26	3.96	0.13	3500	5.2	-1
2M16445239+3644423	3600	5.01	-0.61	1.19	6.59	6.99	0.11	3600	5	-0.6
2M16470934+3657361	3784	5.07	-0.58	1	5.94	5.19	0.08	3800	4.9	-0.6
2M16495034+4745402	3757	4.7	-0.01	0.62	5.92	3.86	0.24	3800	4.7	0
2M16535528+1138453	4062	4.79	0.2	0	4.97	8.32	0.13	4000	4.7	0.2
2M16541202+1154529	3794	4.62	-0.56	0	5.78	5.13	0.11	3800	4.8	-0.4
2M16565961+1133582	3486	5.2	-0.76	1.52	7.14	0	0.08	3500	5.1	-0.8
2M16593773+1155377	3910	4.5	-0.26	0.84	5.39	4.29	0.05	3900	4.7	-0.2
2M17014341+1119582	3767	5.05	-0.51	1.17	5.99	1.72	0.05	3800	4.9	-0.6
2M17190292+2340254	3854	4.72	-0.16	0	5.6	5.64	0.05	3900	4.7	-0.2
2M17331825+3402191	3976	4.75	-0.39	0.39	5.22	3.6	0.03	4000	4.7	-0.4
2M17362594+6820220	3499	4.69	-0.22	0.97	6.91	5.37	0.03	3500	4.8	-0.2
2M17403275+7256146	3991	4.74	-0.32	0.15	5.17	4.7	0.08	4000	4.7	-0.4
2M17480236+7436562	3205	5	-0.18	1	8.32	5.94	0.12	3200	5	-0.2
2M17491402+4823093	3893	4.77	-0.32	0	5.48	4.41	0.08	3900	4.8	-0.4
2M17541820+4758412	3722	4.6	-0.43	1.31	6.04	4.57	0.04	3700	4.7	-0.2
2M17592886+0318233	3895	4.7	-0.04	0	5.46	4.72	0.12	3900	4.7	0
2M18055545+0316213	3574	4.61	0	0	6.6	3.69	0.08	3600	4.7	0
2M18071735+7402564	3950	4.64	-0.1	0	5.28	5.97	0.07	3900	4.7	0
2M18161819+0131277	3505	5.03	-0.42	0.99	6.98	4.53	0.15	3500	5	-0.4
2M18244689-0620311	3484	4.85	-0.15	1.28	7.01	6.05	0.14	3500	4.9	-0.2
2M18254864-0258170	3833	4.66	-0.01	0	5.66	5.3	0.11	3900	4.7	0
2M18415473+0651285	3467	4.85	-0.11	0.69	7.08	6.12	0.09	3500	4.9	-0.2
2M18424666+5937499	3526	4.83	-0.63	1.51	6.83	4.44	0.04	3500	4.9	-0.4
2M18424688+5937374	3536	4.86	-0.69	1.64	6.8	5.41	0.04	3500	4.9	-0.4
2M18451027+0620158	3836	4.78	-0.16	0	5.67	5.08	0.22	3900	4.7	-0.2
2M18543080+4823277	3837	4.99	-0.19	0.9	5.72	3.64	0.05	3900	4.8	-0.4
2M18545777+4730586	3862	4.75	-0.14	0	5.57	5.33	0.03	3900	4.7	-0.2
2M18561502+0449049	3707	4.77	-0.78	1.53	6.12	5.04	0.04	3700	4.9	-0.6
2M18562628+4622532	3304	5.15	-0.25	1.55	7.91	5.91	0.12	3300	5	-0.2
2M18571939+0523084	3670	4.52	-0.22	0.35	6.22	3.94	0.04	3700	4.7	-0.2
2M19004176+0310312	3516	4.97	-0.83	1.65	6.91	4.95	0.05	3500	5	-0.6
2M19010098+4522386	3389	4.87	-0.01	0.96	7.42	3.75	0.06	3400	4.8	0
2M19034293+3831155	3680	4.77	-0.01	0.19	6.21	3.48	0.05	3700	4.7	0
2M19121128+4316106	3616	4.76	-0.67	1.5	6.45	6.09	0.04	3600	4.8	-0.4
2M19165526+0510086	3576	4.68	-0.01	0.5	6.6	2.74	0.02	3600	4.7	0
2M19213157+4317347	3889	4.7	-0.23	0.21	5.48	3.78	0.04	3900	4.7	-0.2
2M19244433+2621167	4170	4.52	-0.04	0	4.65	5.22	0.13	4000	4.7	0
2M19250941+1829397	4074	4.79	-0.29	0	4.94	6.97	0.08	4000	4.7	-0.4
2M19263973+1736418	3499	5.07	-0.38	1.14	7.02	5.68	0.07	3500	5	-0.4
2M19272432+2619292	3593	5.09	-0.37	1.03	6.66	5.96	0.12	3600	4.9	-0.4
2M19301917+3722350	3854	4.69	0.02	0.01	5.59	1.92	0.05	3900	4.7	0
2M19302719+1723396	3667	4.69	-0.02	0.45	6.25	6.84	0.1	3700	4.7	0
2M19312949+4103513	4077	4.74	0.06	0	4.92	3.74	0.06	4000	4.7	0
2M19313868-0658253	3572	4.91	-0.11	0.44	6.66	5.2	0.1	3600	4.8	-0.2
2M19324633-0652178	3489	4.67	-0.22	0.73	6.95	4.78	0.1	3500	4.8	-0.2
2M19325604+1723567	3621	4.73	-0.66	1.41	6.43	5.05	0.04	3600	4.8	-0.4
2M19341617+2553535	3530	4.71	-0.67	1.1	6.79	3.58	0.07	3500	4.9	-0.4
2M19383321+3230175	3496	4.89	-0.2	0.83	6.97	3.46	0.05	3500	4.9	-0.2
2M19390444+2424089	3498	4.9	-0.21	0.88	6.96	4.04	0.21	3500	4.9	-0.2
2M19395886+3950530	3690	4.84	-0.24	0.72	6.19	4.23	0.1	3700	4.8	-0.2
2M19412775+3239512	3626	4.76	-0.71	1.56	6.42	3.97	0.08	3600	4.8	-0.4
2M19420033+4038302	3894	4.68	-0.14	0	5.46	6.32	0.05	3900	4.7	-0.2
2M19454969+3223132	3688	4.95	-0.52	0.82	6.23	3.75	0.12	3700	4.9	-0.6
2M19482428+3250327	3608	4.82	-0.75	1.64	6.5	5.48	0.07	3600	4.9	-0.6
2M19485718+5015245	3476	5.2	-0.3	1.49	7.18	7	0.08	3500	5	-0.4

Table D.1. continued.

APOGEE_ID	iSpec Output							Normalization		
	T_{eff}	$\log g$	[M/H]	v_{mic}	v_{mac}	$v \sin i$	χ^2	T_{eff}	$\log g$	[M/H]
2M19533423+0503410	3691	5.02	-0.75	1.21	6.25	3.7	0.08	3700	4.9	-0.8
2M19541829+1738289	3301	5.1	-0.46	1.79	7.9	8.15	0.12	3300	5	-0.4
2M19543665+4357180	3969	4.76	-0.4	0.36	5.24	4.52	0.03	4000	4.7	-0.4
2M19544358+1801581	1950	4.9	0.29	2.08	16.22	5.42	0.31	2300	5.1	0.4
2M19585332+0522081	3955	4.93	-0.51	0.3	5.33	3.82	0.1	4000	4.8	-0.6
2M20015056+4500500	3474	4.97	-0.08	0.85	7.09	5.81	0.1	3500	4.9	-0.2
2M20024041+3109447	3593	4.93	-0.23	0.95	6.59	5.2	0.07	3600	4.8	-0.2
2M20032651+2952000	3292	5.07	-0.19	1.07	7.93	1.87	0.05	3300	5	-0.2
2M20053276+3039324	3870	4.57	-0.44	1.2	5.53	5.66	0.04	3900	4.7	-0.4
2M20122244+2043113	3605	4.99	-0.7	1.57	6.57	5.4	0.11	3600	4.9	-0.6
2M20162519+5621561	3665	4.67	0	0	6.25	4.96	0.05	3700	4.7	0
2M20185746+2704165	3764	5.07	-0.43	0.73	6.01	5.07	0.06	3800	4.9	-0.6
2M20202082+2837583	3780	4.79	0.01	0	5.86	4.53	0.1	3800	4.7	0
2M20291663+4507525	3702	4.76	-0.17	0.51	6.13	2.08	0.09	3700	4.8	-0.2
2M20331096+4553299	3587	4.93	-0.35	0.85	6.62	5.09	0.07	3600	4.9	-0.4
2M20584898+5115421	3593	4.93	-0.23	0.75	6.59	4.4	0.12	3600	4.8	-0.2
2M21003448+5156016	3495	4.88	-0.24	1.08	6.97	4.73	0.14	3500	4.8	-0.2
2M21013304+4046208	3503	4.98	-0.48	1.14	6.97	5.59	0.07	3500	4.9	-0.4
2M21074857+2945266	3587	4.95	-0.39	0.9	6.62	3.31	0.09	3600	4.9	-0.4
2M21140743+4924350	3507	5.02	-0.45	1.01	6.97	4.42	0.06	3500	5	-0.4
2M21232573+6734153	3557	5.3	-0.54	0.89	6.91	0	0.08	3600	5.1	-0.8
2M21281491+4654126	3886	4.69	0	0	5.49	4.22	0.12	3900	4.7	0
2M21400112+5408179	3593	5.03	-0.56	1.32	6.63	4.34	0.14	3600	5	-0.6
2M21402935+5400301	3503	4.86	-0.46	1.19	6.93	6.57	0.14	3500	4.9	-0.4
2M21474194+5341222	3677	4.64	-0.13	0.02	6.2	4.3	0.07	3700	4.7	-0.2
2M21561443+3943468	3478	5.3	-0.31	1.24	7.23	4.37	0.1	3500	5	-0.4
2M21573509+5026323	3196	4.95	-0.02	1.03	8.34	5	0.12	3200	4.9	0
2M22010861+4901108	3967	4.67	-0.07	0	5.23	4.42	0.14	4000	4.7	0
2M22563497+1633130	3802	4.68	0.01	0	5.76	6.38	0.04	3800	4.7	0
2M23034347+6524293	3295	4.93	-0.01	1.06	7.86	4.76	0.07	3300	4.9	0
2M23062184+650326	3436	4.77	-0.8	1.27	7.19	5.53	0.09	3400	5	-0.6
2M23110137+4653414	3475	4.92	-0.14	1.11	7.06	6.44	0.09	3500	4.8	-0.2
2M23134861+1227072	3570	5.06	0.02	0.65	6.73	3.31	0.05	3600	4.8	0
2M23165396+6109419	3773	4.9	-0.39	1.45	5.91	3.28	0.06	3800	4.8	-0.4
2M23171589+6110496	3574	4.86	-0.01	0.53	6.64	4.66	0.08	3600	4.8	0
2M23175293+6109518	3768	5.08	-0.5	1.02	6	2.47	0.06	3800	4.9	-0.6
2M23200542+6356068	3679	4.64	-0.01	0.2	6.2	2.57	0.07	3700	4.7	0
2M23205304+1205009	3592	4.98	-0.6	1.04	6.61	4.02	0.06	3600	4.9	-0.6
2M23212582+6547582	3689	5.07	-0.56	1.16	6.28	5.34	0.08	3700	4.9	-0.6
2M23230603+6211124	3821	4.98	-0.21	1.19	5.78	4.26	0.04	3900	4.8	-0.4
2M23460112+7456172	3772	5.4	-0.72	1.3	6.17	0	0.07	3800	5	-1
2M23592772+1630288	3389	4.93	0.04	0.76	7.44	3.98	0.05	3400	4.8	0
2M23592810+7506017	3909	4.68	-0.04	0	5.41	4.76	0.06	3900	4.7	0
2M23595589+1508091	3761	5.09	-0.41	0.74	6.03	1.74	0.05	3800	4.9	-0.6